

SANDIA REPORT

SAND2022-0583

Printed January 2022

**Sandia
National
Laboratories**

Probabilistic Modeling of Climate Change Impacts on Renewable Energy and Storage Requirements for NM's Energy Transition Act

Clifford K. Ho, Erika L. Roesler, Tu Nguyen, and James Ellison

Prepared by
Sandia National Laboratories
Albuquerque, New Mexico
87185 and Livermore,
California 94550

Issued by Sandia National Laboratories, operated for the United States Department of Energy by National Technology & Engineering Solutions of Sandia, LLC.

NOTICE: This report was prepared as an account of work sponsored by an agency of the United States Government. Neither the United States Government, nor any agency thereof, nor any of their employees, nor any of their contractors, subcontractors, or their employees, make any warranty, express or implied, or assume any legal liability or responsibility for the accuracy, completeness, or usefulness of any information, apparatus, product, or process disclosed, or represent that its use would not infringe privately owned rights. Reference herein to any specific commercial product, process, or service by trade name, trademark, manufacturer, or otherwise, does not necessarily constitute or imply its endorsement, recommendation, or favoring by the United States Government, any agency thereof, or any of their contractors or subcontractors. The views and opinions expressed herein do not necessarily state or reflect those of the United States Government, any agency thereof, or any of their contractors.

Printed in the United States of America. This report has been reproduced directly from the best available copy.

Available to DOE and DOE contractors from

U.S. Department of Energy
Office of Scientific and Technical Information
P.O. Box 62
Oak Ridge, TN 37831

Telephone: (865) 576-8401
Facsimile: (865) 576-5728
E-Mail: reports@osti.gov
Online ordering: <http://www.osti.gov/scitech>

Available to the public from

U.S. Department of Commerce
National Technical Information Service
5301 Shawnee Rd
Alexandria, VA 22312

Telephone: (800) 553-6847
Facsimile: (703) 605-6900
E-Mail: orders@ntis.gov
Online order: <https://classic.ntis.gov/help/order-methods/>



ABSTRACT

This report provides a study of the potential impacts of climate change on intermittent renewable energy resources, battery storage, and resource adequacy in Public Service Company of New Mexico's Integrated Resource Plan for 2020 – 2040. Climate change models and available data were first evaluated to determine uncertainty and potential changes in solar irradiance, temperature, and wind speed in NM in the coming decades. These changes were then implemented in solar and wind energy models to determine impacts on renewable energy resources in NM. Results for the extreme climate-change scenario show that the projected wind power may decrease by ~13% due to projected decreases in wind speed. Projected solar power may decrease by ~4% due to decreases in irradiance and increases in temperature in NM. Uncertainty in these climate-induced changes in wind and solar resources was accommodated in probabilistic models assuming uniform distributions in the annual reductions in solar and wind resources. Uncertainty in battery storage performance was also evaluated based on increased temperature, capacity fade, and degradation in round-trip efficiency. The hourly energy balance was determined throughout the year given uncertainties in the renewable energy resources and energy storage. The loss of load expectation (LOLE) was evaluated for the 2040 No New Combustion portfolio and found to increase from 0 days/year to a median value of ~2 days/year due to potential reductions in renewable energy resources and battery storage performance and capacity. A rank-regression analyses revealed that battery round-trip efficiency was the most significant parameter that impacted LOLE, followed by solar resource, wind resource, and battery fade. An increase in battery storage capacity to ~25,000 – 30,000 MWh from a baseline value of ~14,000 MWh was required to reduce the median value of LOLE to ~0.2 days/year with consideration of potential climate impacts and battery degradation.

ACKNOWLEDGEMENTS

The authors thank Nick Phillips from PNM for providing data and consultation regarding this work. This work was funded by the Climate Change Security Center program (278/40.02.01.04.02.01.06) at Sandia National Laboratories (Center 8900).

This report was prepared as an account of work sponsored by an agency of the United States Government. Neither the United States Government nor any agency thereof, nor any of their employees, makes any warranty, express or implied, or assumes any legal liability or responsibility for the accuracy, completeness, or usefulness of any information, apparatus, product, or process disclosed, or represents that its use would not infringe privately owned rights. Reference herein to any specific commercial product, process, or service by trade name, trademark, manufacturer, or otherwise does not necessarily constitute or imply its endorsement, recommendation, or favoring by the United States Government or any agency thereof. The views and opinions of authors expressed herein do not necessarily state or reflect those of the United States Government or any agency thereof.

Sandia National Laboratories is a multimission laboratory managed and operated by National Technology and Engineering Solutions of Sandia, LLC., a wholly owned subsidiary of Honeywell International, Inc., for the U.S. Department of Energy's National Nuclear Security Administration under contract DE-NA0003525.

CONTENTS

1. Introduction and Objectives	9
1.1. Background and Problem Statement	9
1.2. Objectives	9
1.3. Overview of Report.....	10
2. Climate Change Modeling.....	11
2.1. Climate Data Source and Methods.....	11
2.2. Results and Discussion.....	14
2.3. Comparison with Other Studies	16
2.4. Next Steps.....	17
3. Climate Change Impacts on Solar and Wind Power Generation	19
3.1. Wind and Solar Resources in New Mexico.....	19
3.2. Impact of Modeled Climate Change on PNM Wind Power Generation.....	19
3.2.1. Methodology.....	19
3.3. Impact of Modeled Climate Change on PNM Solar Power Generation.....	21
3.3.1. Climate Scenario Selection.....	21
3.3.2. Methodology – Specific Method.....	22
3.3.3. Methodology – General Method	23
4. Climate Change Impacts on Battery Storage	25
4.1. Impact of Temperature Change on Battery Storage.....	25
4.2. Impacts of Capacity Fade and Round-Trip Efficiency on Battery Storage.....	27
4.3. Implementation into QuEST.....	28
5. Probabilistic Analysis of Climate Change Impacts and Battery Performance	29
5.1. Modeling Approach.....	29
5.1.1. Uncertainty in Wind Energy Resources.....	31
5.1.2. Uncertainty in Solar Energy Resources.....	33
5.1.3. Uncertainty in Battery Storage Resources	34
5.1.4. Annual Energy Load.....	35
5.2. Modeling Results.....	36
6. Conclusion and Recommendations.....	41
6.1. Climate Modeling.....	41
6.2. Climate Impacts on Wind and Solar Energy Resources	41
6.3. Climate Impacts on Battery Performance and Storage	41
6.4. Energy Balance and Climate Impacts on LOLE.....	42

LIST OF FIGURES

Figure 1. PNM 2040 portfolios for carbon-free electricity production in 2040 [1]......	9
Figure 2. Contour plots of the annual mean of the entire simulation from the E3SM CMIP5 data. Top to bottom are the ‘No Climate Change’ (ECA_piControl), ‘Low Climate Change’ (historical), and ‘High Climate Change’ (SSP585) simulations. Variables of interest for this study included (left to right) Surface Downwelling Shortwave Radiation, Surface Temperature, and Near-Surface Wind Speed.....	12
Figure 3. Time series of the surface downwelling shortwave radiation, surface temperature, and near-surface wind speed for the ‘No Climate Change’ (ECA_piControl), ‘Low	

	Climate Change’ (historical), ‘High Climate Change’ (SSP585) CMIP6 E3SM simulations for global, contiguous United States, and New Mexico areas. The time series represents monthly means from the simulation data, and the data were smoothed by applying a 48-point running average.	14
Figure 4.	Probability Distribution Functions of the time-averaged and spatially-averaged (over New Mexico) of (top to bottom) surface downwelling shortwave radiation, surface temperature, and near-surface wind speed for the three simulations scenarios in the CMIP6 E3SM database.....	15
Figure 5.	Power Curve for IEC Class II Turbine	20
Figure 6.	Cumulative distribution functions of climate-induced changes in wind and solar resources (top) and uncertainty in battery performance (RTE and capacity fade; bottom).....	31
Figure 7.	Plot of historical average capacity factors for PNM wind energy resources by hour and month (2013 – 2019) [1].....	32
Figure 8.	Plot of historical average capacity factors for PNM solar energy resources by hour and month (2013 – 2019) [1].....	34
Figure 9.	Cumulative probability of loss of load expectation (LOLE) with inclusion of solar and wind resource uncertainty resulting from climate change and uncertainty in battery performance. Uniform distributions of $\pm 25\%$ (top) and $\pm 50\%$ (bottom) were assumed for the solar, wind, and battery performance uncertainty distributions.	37
Figure 10.	Impact of uncertainties in solar and wind resources and battery performance resulting from climate change on LOLE. Standardized rank regression coefficients are shown. Uniform distributions of $\pm 50\%$ were assumed for the solar, wind, and battery performance uncertainty distributions.	38
Figure 11.	Impact of uncertainties in solar and wind resources and battery performance resulting from climate change on LOLE variability. Incremental coefficients of determination are shown. Uniform distributions of $\pm 50\%$ were assumed for the solar, wind, and battery performance uncertainty distributions.	38
Figure 12.	Cumulative probability of LOLE with increased battery storage capacity of 100,000 MWh (from 14,328 MWh) resulting in a 95% confidence that the LOLE would be ≤ 0.2 days/year for assumed uncertainties in solar, wind, and battery performance.	39

LIST OF TABLES

Table 1.	Description of data sources from simulations used for three climate change scenarios over New Mexico.....	11
Table 2.	List of Variables for used to determine resources uncertainty for solar, wind, and battery.	13
Table 3.	Averages and Standard Deviations of solar radiation, surface temperature, and surface wind from E3SM CMIP6 scenarios.....	16
Table 4.	Wind Resources in New Mexico.....	19
Table 5.	List of PRC-approved and pending-approval large solar arrays in New Mexico.....	19
Table 6.	IEC Wind Turbine Classes.....	20
Table 7.	Solar PV Scenarios and Results.....	23
Table 8.	Parameters used in HVAC modeling of BESS power consumption.....	25

Table 9. Modeled annual HVAC energy consumption as a function of ambient temperature rise.	27
Table 10. Summary of firm fixed resources assumed for PNM 2040 No New Combustion scenario (in addition to solar and wind generation) [1].	29
Table 11. Summary of uncertainty distributions in probabilistic simulations.	30
Table 12. Historical average capacity factors for PNM wind energy resources (2013 – 2019) [1].	32
Table 13. Hourly baseline wind generation (MW) based on capacity factors in Table 12 and total prescribed wind generation capacity of 956 MW in the PNM IRP 2040 No New Combustion portfolio [1].	33
Table 14. Historical average capacity factors for PNM solar energy resources (2013 – 2019) [1].	33
Table 15. Hourly baseline solar generation (MW) based on capacity factors in Table 14 and total prescribed solar generation capacity of 3,165 MW in the PNM IRP 2040 No New Combustion portfolio [1].	34
Table 16. Summary of planned battery storage systems in PNM’s No New Combustion, most cost-effective portfolio [1].	35
Table 17. Average hourly loads (MW)* by month using reference 2040 forecast (PNM 2020 – 2040 IRP [1]).	35

This Page Left Blank

1. INTRODUCTION AND OBJECTIVES

1.1. Background and Problem Statement

In January 2021, the Public Service Company of New Mexico (PNM) issued its fifth Integrated Resource Plan (IRP), “PNM 2020-2040 Integrated Resource Plan,” which included carbon-free electricity generation portfolios by 2040 [1]. PNM is a regulated utility and NM’s largest energy provider with currently over 500,000 residential and business customers and ~3 GW of generation capacity. The PNM 2020-2040 IRP included portfolios to meet NM’s Energy Transition Act, which requires 100% of electricity generation to be carbon free by 2045. PNM intends to meet that goal by 2040 and includes two different portfolios: a Technology Neutral scenario that includes hydrogen combustion turbines (initially powered by natural gas through the 2020s), and a No New Combustion scenario that relies primarily on solar, wind, and battery storage (Figure 1).

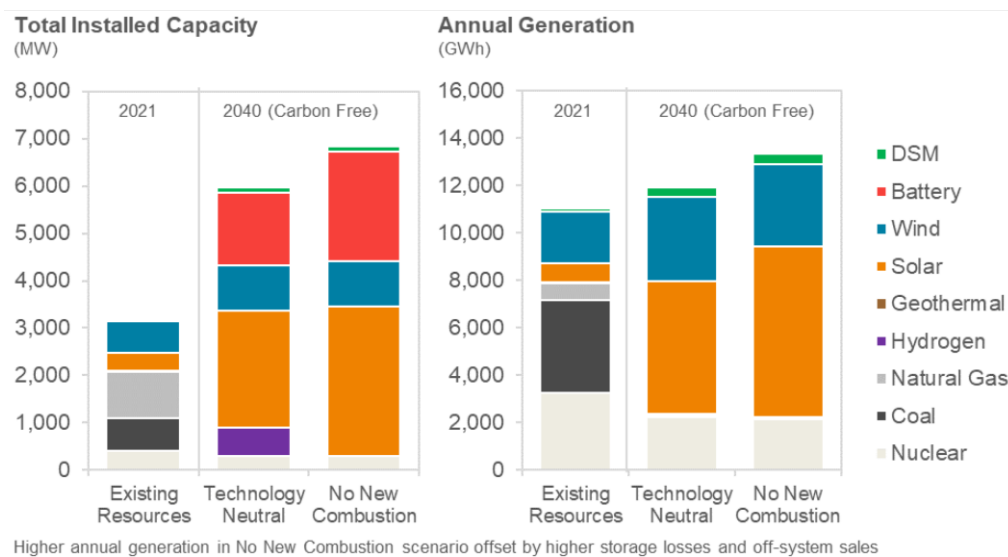


Figure 1. PNM 2040 portfolios for carbon-free electricity production in 2040 [1].

In the PNM 2020-2040 IRP, treatment of uncertainty and sensitivity analyses focused primarily on demand-side uncertainty. Climate change and potential impacts on intermittent wind and solar resources were not considered. In addition, uncertainties in large-scale, long-term performance and reliability of battery storage systems were not considered; the battery storage system was assumed to operate at nameplate capacity for its entire 20-year lifetime (due to contracted maintenance and servicing of the systems).

1.2. Objectives

The objectives of this study were to develop a probabilistic model and framework to evaluate inherent uncertainties in the energy resources and storage assumed in the PNM 2020-2040 IRP:

- Long-term changes in solar and wind resources caused by climate change
- Uncertainties in battery performance caused by capacity fade, degradation in round-trip efficiency, and long-term temperature increase caused by climate change
- Impact on the annual loss of load expectation (LOLE) and required energy storage

Probabilistic models were developed to evaluate the hourly energy balance each year given uncertainties in the renewable energy resources and energy storage. The loss of load expectation (LOLE) was probabilistically evaluated for the 2040 No New Combustion portfolio considering potential reductions in renewable energy resources and battery storage.

1.3. Overview of Report

Section 2 presents the climate data and methods that were used to determine potential climate-change impacts on solar irradiance, temperature, and wind speeds. Wind and solar resources are evaluated, and comparisons with other climate models are presented. Section 3 then evaluates the impact of the modeled climate change on PNM wind and solar power generation. Section 4 describes modeling to evaluate the potential impacts of climate change (increased temperatures), capacity fade, and round-trip efficiency degradation on battery performance. Section 5 describes a probabilistic model to evaluate the hourly energy balance with consideration of the inherent uncertainties in solar and wind resources, power generation, and battery storage on LOLE. Finally, Section 6 provides conclusions and recommendations for follow-on work.

2. CLIMATE CHANGE MODELING

2.1. Climate Data Source and Methods

Three simulations from the Department of Energy’s Energy Exascale Earth System Model (E3SM) were chosen from the Earth System Grid Federation Climate Model Intercomparison Project – version 6 (CMIP6) repository [2-5]. The CMIP6 simulation set contains output contributed from Earth system modeling centers. This set includes simulations representing the Earth system response under various, prescribed forcing scenarios. For this study, the three simulations chosen were a baseline simulation called pre-industrial control (piControl), a moderately warming simulation called historical, and a highly warming simulation called SSP585. The three simulations were from the ‘r1i1p1f1’ variant identification, meaning the first realization, first initialization, and same physics and forcing. The data were all written in the form of monthly averages with more details below.

The baseline simulations include prescribed greenhouse gas concentrations, such as CO₂, set to values at a time in human history where anthropogenic signatures were not distinguishable on the temperature of the atmosphere. These baseline simulations start in the year 1850 and usually run with that concurrent year, 1850, for several hundred years. The purpose of the duration of these simulations is to emulate the Earth system climate variability and seasonality so that statistically significant values for a baseline, unperturbed Earth, can be compared against a simulated earth with increasing anthropogenic signatures such as increasing greenhouse gas concentrations. Table 1 lists the description of data used for the Preindustrial control, baseline data. Because this data set has no induced warming on the Earth system, it was also referred to as the ‘no climate change’ scenario for this work.

The historical simulation dataset, also described in Table 1, uses CO₂ concentrations prescribed or calculated from years 1850 to 2014. The Earth system will be warming due to increased greenhouse gas concentration build-up over this time period, so this dataset was referred to as the ‘low climate change’ scenario. The last simulation dataset used is called SSP585. It was developed as an update of the high-emission ‘business as usual’ IPCC RCP8.5 scenario [2, 5]. This dataset has the highest amount of warming of the three and is called ‘high climate change’ in this work.

Table 1. Description of data sources from simulations used for three climate change scenarios over New Mexico.

Scenario	Data and Simulation Description
No Climate Change	<ul style="list-style-type: none"> - ECA version of Preindustrial control simulation - CR-1.7 CMIP-6.2, ScenarioMIP - Concurrent year 1850 year for 165 years, monthly averages
Low Climate Change	<ul style="list-style-type: none"> - Update of RCP8.5 based on SSP5 - CR-1.7 CMIP-6.2, ScenarioMIP - Jan 1850 - Dec 2014, monthly averages
Extreme Climate Change	<ul style="list-style-type: none"> - Update of RCP8.5 based on SSP5 - CR-1.7 CMIP-6.2, ScenarioMIP - 1032 monthly-averaged time points, Jan 2015-Dec 2021

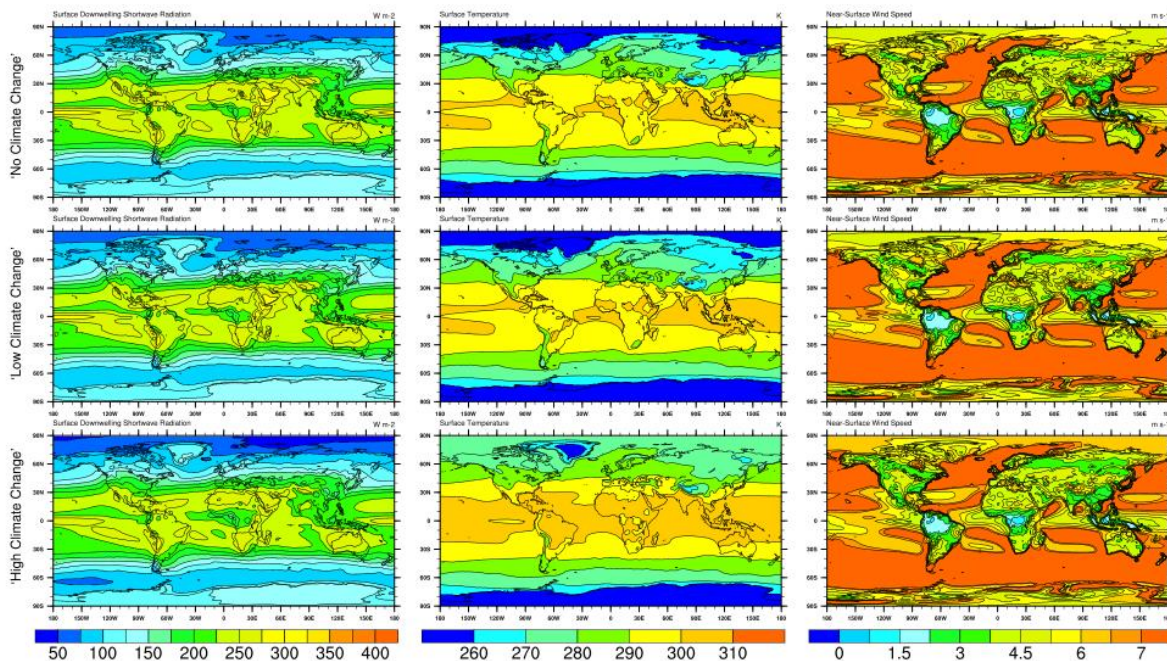


Figure 2. Contour plots of the annual mean of the entire simulation from the E3SM CMIP5 data. Top to bottom are the ‘No Climate Change’ (ECA_piControl), ‘Low Climate Change’ (historical), and ‘High Climate Change’ (SSP585) simulations. Variables of interest for this study included (left to right) Surface Downwelling Shortwave Radiation, Surface Temperature, and Near-Surface Wind Speed.

The variables chosen for analysis are fundamental variables influencing wind energy production, solar energy production, and battery storage efficiency. Table 2 lists the variables chosen from the E3SM CMIP6 database. For wind power generation, power is a function of wind speed cubed. The variable for near surface wind, `sfcWind`, was used instead of wind at hub height. ‘`sfcWind`’ is stated to be the wind at about 10 meters off the ground surface. It should be noted that the wind speed within the boundary layer generally follows a log wind profile as the surface frictional effects are less impactful as you move away from the surface. Therefore, any additional low level increase in height – 10s to 100s of meters will give ‘generally’ an increase in wind speed and therefore power. This variable was readily available and required no additional data processing after downloading.

Solar energy production from solar installations relies on direct and diffuse solar radiation. The potential for solar energy production is computed from the Global Horizontal Irradiance (GHI), which is the sum of Diffuse Horizontal Irradiance (DHI) and Direct Normal Irradiance (DNI) multiplied by the cosine of the solar zenith angle (z), $GHI = DHI + DNI \cdot \cos(z)$. Given radiation parameterizations in earth system models are column-based physics with no radiation interaction between columns, the surface downwelling shortwave radiation is associated with the needed GHI variable. Clear-sky shortwave radiation at the surface from climate models is DNI, but the diffuse radiation that could be scattered equally in all directions from molecules, aerosols, and clouds is more difficult to ascertain from earth system model output. Ground reflectance could also be included in GHI, but this contribution is usually low compared to DHI and DNI. It was determined that the variable ‘`rsds`’ would be the most appropriate choice for determining solar variability with a changing climate.

Table 2. List of Variables for used to determine resources uncertainty for solar, wind, and battery.

CMIP6 Variable	Renewable Resource	Description
sfcWind (m s ⁻¹),	Wind power	Near-surface (usually, 10 meters) wind speed in Time, (Latitude, Longitude) (1 degree) (180, 360)
rsds (W m ⁻²),	Solar power	Surface Downwelling Shortwave Radiation in Time, (Latitude, Longitude) (1 degree) (180, 360)
Ts (K),	Battery storage	Surface Temperature in Time, (Latitude, Longitude) (1 degree) (180, 360)

Figure 2 shows the time-averaged global annual mean of the three simulations and the variables of interest, surface downwelling shortwave radiation, surface temperature, and near-surface wind power. These annual averages are shown to give a notional sense of the global variability and magnitudes of the three variables, showing differences in energy, temperature, and wind over New Mexico compared to other regions of the globe. Qualitatively, there is little spatial difference between the ‘No Climate Change’ and ‘Low Climate Change’ scenarios. The ‘High Climate Change’ scenario shows significant warming in the Arctic and in New Mexico. Wind speeds and surface downwelling shortwave radiation over New Mexico do not change as much as temperature across the three scenarios.

The time series trends for each of the variables for each of the simulation is shown in Figure 3. The simulation output is in the form of monthly means, and a 48-point running average was computed for each of the time series. Three area-weighted averages were computed for comparison: the entire globe, the contiguous United States (i.e., lower 48 States), and the State of New Mexico. In the ‘No Climate Change’ scenario, it is expected for there to be little-to-no-trend over the time series because the Earth system is in pre-industrial energy equilibrium. The ‘Low Climate Change’ scenario shows increasing surface temperatures in the latter portion of the simulation, which is consistent with observations and the basis upon which this simulation is designed. The trends in the surface downwelling shortwave radiation and near-surface wind speed also show minute changes in the end of the simulation. Impacts in the simulation of coarse spatial resolution and parameterizations, or not enough forcing to cause a discernable change in the time series are all probably causes for these two variables’ trends. The ‘High Climate Change’ scenario shows the expected increase in surface temperature, a reduction in near-surface wind speed, and no discernable change in the surface downwelling shortwave radiation. There is little confidence in the trends of wind and radiation for this scenario, with more discussion given in Section 2.3.

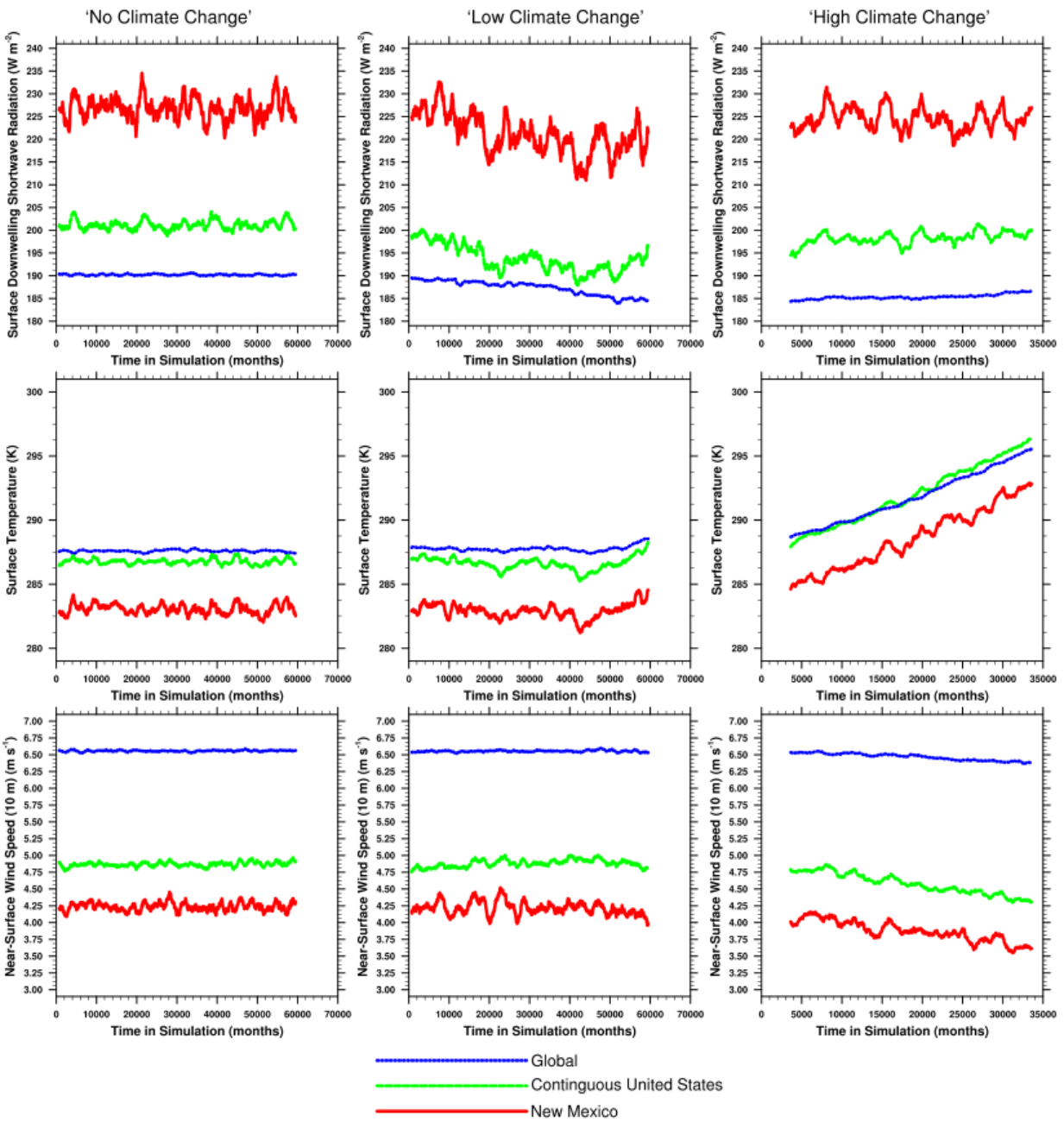


Figure 3. Time series of the surface downwelling shortwave radiation, surface temperature, and near-surface wind speed for the 'No Climate Change' (ECA_piControl), 'Low Climate Change' (historical), 'High Climate Change' (SSP585) CMIP6 E3SM simulations for global, contiguous United States, and New Mexico areas. The time series represents monthly means from the simulation data, and the data were smoothed by applying a 48-point running average.

2.2. Results and Discussion

Bounds and trends are needed for the solar and wind resource calculations. Because climate models are inherently uncertain in that they are and represent chaotic systems with much dependence on

initial conditions for solutions, it was decided to take averages of the three simulations over the state of New Mexico. New Mexico's land area is small compared to the global surface, and instances of the climate over New Mexico for any given month could be representative of the past, current, and future climate. Table 3 shows the time averages and standard deviations over New Mexico for the entire simulations for the three variables. Figure 4 shows the probability distribution functions for the time series averaged over New Mexico for each of the variables in each simulation scenario.

From Table 3, there is no trend in surface downwelling shortwave radiation (i.e., solar radiation) over the 'No', 'Low', and 'High' climate change scenarios. The near-surface wind decreases slightly from 'No' to 'High' climate change scenarios, and the temperature increases by 5 K from 'No' to 'High' climate change.

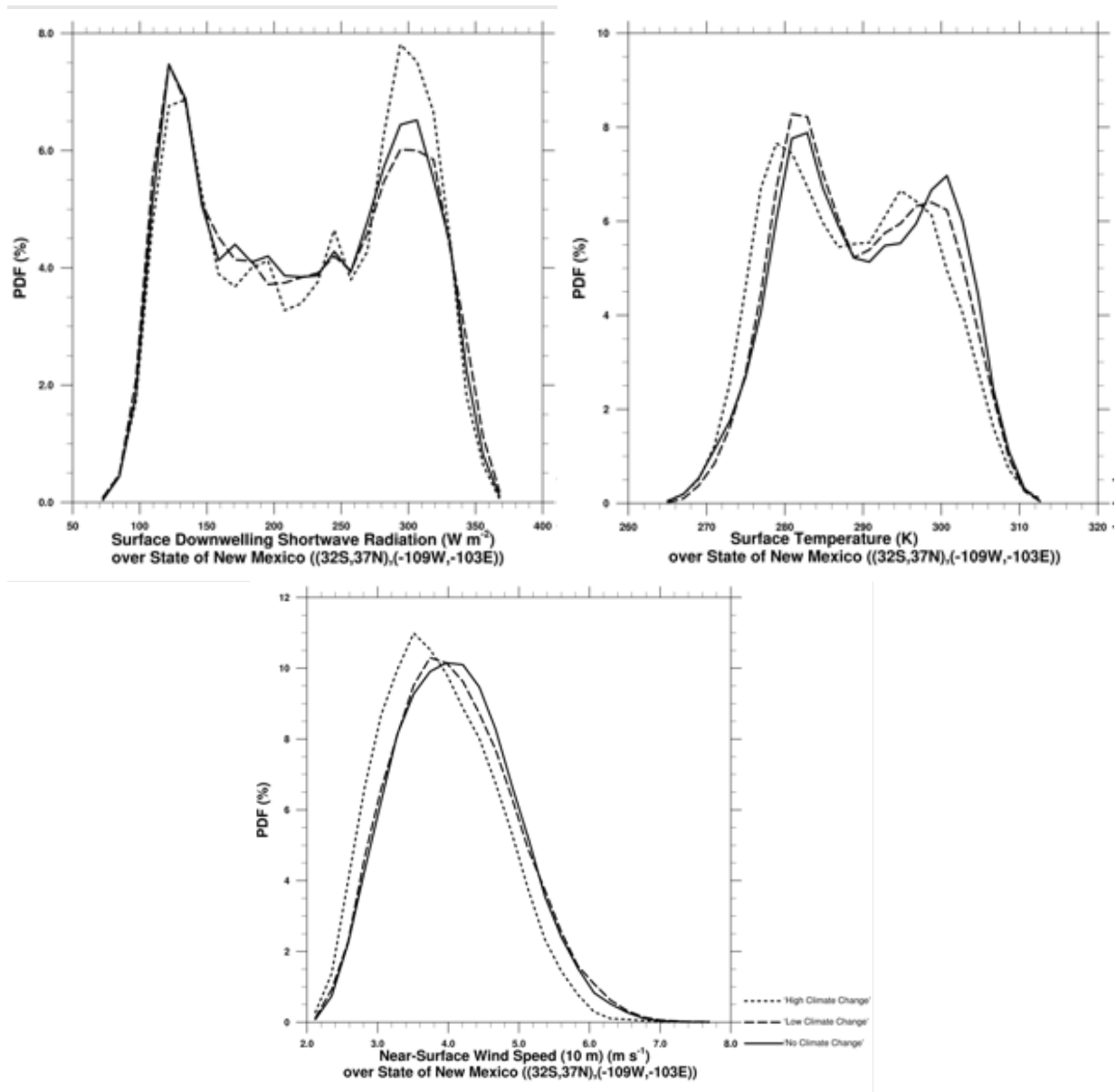


Figure 4. Probability Distribution Functions of the time-averaged and spatially-averaged (over New Mexico) of (top to bottom) surface downwelling shortwave radiation, surface temperature, and near-surface wind speed for the three simulations scenarios in the CMIP6 E3SM database.

Table 3. Averages and Standard Deviations of solar radiation, surface temperature, and surface wind from E3SM CMIP6 scenarios.

Variable	Scenario	Average	Standard Deviation
Solar, $rsds$ ($W m^{-2}$)	No climate change	226.7	75.21
	Low climate change	221.0	76.51
	High climate change	224.4	75.56
Surface Temperature, T_s (K)	No climate change	283.0	9.250
	Low climate change	283.1	9.244
	High climate change	288.5	9.613
Surface Wind, $sfcWind$ ($m s^{-1}$)	No climate change	4.239	0.7831
	Low climate change	4.215	0.8471
	High climate change	3.871	0.8012

2.3. Comparison with Other Studies

This study is not alone in assessing climate change impacts on renewable energy resources. Global, national, and regional bodies of research exist for specific technologies as well as system-level studies. For future reference, Solaun & Cerdá [6] provides global overviews of climate change effects on renewable resources. Additionally, a nationwide assessment of energy demand under different emissions scenarios stated that electricity demand will increase on average of 10%, which included power system generation with power system planning and operations [7]. In the literature review performed for this study, it was found that there is unanimous uncertainty in the magnitude and direction of energy resources being impacted regionally and under different future climate scenarios. The focus now narrows to literature that has the most direct application or comparison with this work, this section provides an overview of select literature reporting for the southwestern United States. For neighboring state Texas for solar and wind, wind increases by 1-4%, but there is no clear concurrence on solar production for future years 2041-2050 [8, 9].

Wind power, although very specific to region, show both an increase and decrease in potential wind energy production through the variability of wind speed projections over different seasons and emissions scenarios [8-10]. Often, a higher-resolved North American regional atmospheric model such as the NACORDEX (North American component of the international CORDEX (Coordinated Regional Downscaling Experiment) [11], or WRF (Weather Research and Forecasting model) [12] is used in these studies and compared with a courser resolution global model [13]. Recently there have been observations that winds, including surface winds, are slowing globally. A recent review paper suggests that the data supporting this claim might be region-specific, and more information about internal modes of climate and changes to land use, land cover is needed before understanding this theoretical trend [14]. The previous works considered for comparison here did not mention the observational trend of wind stillness in their findings.

For solar power, there appears to be no agreement that solar resources will increase or decrease for a given future, warmer climate across the western United States [10, 15-18]. Even comparisons using 37 Earth system models run under the CMIP5 protocols showed an increase in solar production for the southern United States. However, when 14 regional climate models (i.e., higher spatial

resolution) were used, the solar production was calculated to decrease [19]. Although unresolved cloud behavior seems to be a likely culprit in explaining the differences between the global and regional models, differences in cloud properties alone could not explain differences, so it was assumed aerosols were also playing a role with an approximately $\pm 2.5\%$ change in solar radiation at the surface. However, it should be noted that aerosol concentrations and pathways contain high uncertainty and speculation in future climate projections.

For general climate model bias as it relates to observations, climate modelling groups publish simulated model bias compared to global observations. The climate model used in this work, E3SM, has reported a negative bias of shortwave (visible) cloud radiative effects compared to observations, but with little to no precipitation bias compared to global satellite observations. This could imply that E3SM rains-out the simulated cloud, leaving too-little cloud mass after a precipitation event. Additionally, E3SM has a strong aerosol-related effective radiative forcing and a high equilibrium climate sensitivity. This means the SSP585 scenario is likely to project a warmer Earth than other models at the end of the simulation in year 2100.

2.4. Next Steps

In gathering information needed to compute future climate change scenarios, a list was developed of potential future work that could analyze details of future climate change impacts to renewable energy production.

- Models that have high spatial and temporal resolution produce different trends than global models. Despite high variability and uncertainty, understanding the benefits of additional information at the cost of computer time is still undetermined for New Mexico [9]. Understanding downscaling for this problem is needed.
- In the CMIP6 database, the climate variable standards for solar radiation did not separate the Global Horizontal Irradiance (GHI), into the terms of Diffuse Horizontal Irradiance (DHI) and Direct Normal Irradiance (DNI), $GHI = DHI + DNI \cdot \cos(z)$. Understanding predictions and baseline results of diffuse and direct will help understand model bias in changes in aerosol optical depth and cloud cover.
- The results presented here are monthly means which do not account for nighttime and daytime differences with high time resolved datasets. For solar power production, nighttime values will be different than daytime, and wind production might also change over a diurnal cycle. Finding data in the CMIP6 archive or going to individual model output will clarify the computed answers and could change the uncertainty distribution.
- Wind turbines have cut-in and cut-out speeds. Higher time-resolved values for wind will show when wind speed is too great for turbines.
- Although this is not expected to change the findings of this report, using data from the CMIP6 archive that has more vertical levels, or altitude values, so that hub height and not sfcWind is used to calculate the wind power generation.
- Trends for wind slowing and stillness over New Mexico should be investigated in both observational data and simulated future climate projections.

- The E3SM baseline simulation (i.e., the pre-industrial control) should be compared to reanalysis and other weather-based datasets to improve the understanding of the baseline bias.
- Other studies have used field-acquired data with machine learning sorting algorithms to determine potential weather impacts on renewable energy production [20]. Given the difficulty of earth system models to simulate extremes, linking realistic data with future projections is an area of potential research.
- How can the unresolved clouds, and uncertainty in cloud cover be accounted for? Jiménez et al. [21] looked at 6-hour ensemble simulations with WRF Solar for unresolved cumulus with observations and found that parameterizing radiative effects of deep and shallow cumulus is necessary to reduce a 55% overprediction in GHI. A positive GHI bias has been reported in WRF over Albuquerque, New Mexico [12]. How can this cloud bias be accounted for in global earth system models?
- Other options for increasing resolution include using variable or refined resolution atmospheric models. These configurations could also be linked with Sun4Cast and weather prediction to compute solar variability [17]. Wang et al. [22] used CESM-VR with clustering for wind resources over California and found statistically significant changes in capacity. They found through clustering weather patterns that over a 36-year period, wind regimes occurring on “hot summer days increased at half a day per year and stagnant conditions increased at one-third days per year.” Using downscaled MERRA with WRF and energy firm data helped drive this finding [23].

3. CLIMATE CHANGE IMPACTS ON SOLAR AND WIND POWER GENERATION

3.1. Wind and Solar Resources in New Mexico

Table 4 summarizes the existing wind resources in NM operated by PNM, and Table 5 summarizes the existing and pending solar resources in NM operated by PNM. The older wind turbines are at a hub height of 80 meters, and the newer ones are at 90 meters. PNM will likely add more wind in the future, but the timing and amount are uncertain. Additional wind capacity will probably also be in Torrance County (near Clines Corners) because of access to PNM transmission.

Table 4. Wind Resources in New Mexico.

Existing Wind PPA Resources	County	Net Capacity (MW)	Lat.	Lon.	Turbine Cap (MW)	Turbine Model	Hub Height (m)
NM Wind Energy Center	Quay	200	34.63	-104.05	1.5	GE1.5-87	80
Casa Mesa Wind	Quay	50	34.6	-103.99	2.5	GE2.5-127	89
La Joya 1	Torrance	166	34.62	-105.65	2.5	GE2.5-127	89
La Joya 2	Torrance	140	34.69	-105.34	2.5	GE2.5-127	89
Red Mesa Wind	Sandoval	102	35.26	-107.38	1.6	GE1.6-82.5	80

Table 5. List of PRC-approved and pending-approval large solar arrays in New Mexico.

	AC Capacity (MW)	Latitude	Longitude	Status
Arroyo	300	35.95462	-107.622	PRC-approved
Jicarilla 1	50	36.31675	-107.316	PRC-approved
San Juan	200	36.82913	-108.349	PRC-approved
Rockmont*	100	36.77774	-108.373	PRC-approved
Atrisco	300	35.2007	-106.933	Submitted Application
Jicarilla 2	50	36.238	-107.297	Submitted Application
Sky Ranch	190	34.76835	-106.791	Submitted Application
Encino North	50	35.35457	-106.856	Submitted Application

3.2. Impact of Modeled Climate Change on PNM Wind Power Generation

Using hourly 2012 wind speed data [24] for a point representing the NM Wind Energy Center wind generator (204 MW installed capacity), we found that that a drop of 8.7% in wind speed each hour yielded a 13% drop in total wind energy output for the year. The following sections describe these findings.

3.2.1. Methodology

2012 wind speed data for a site representing the NM Wind Energy Center were obtained on an hourly basis from the Wind Prospector [24]. Specifically, wind speed data for the cell located at lat: 34.65, long -104.04 (Site ID: 874603 on the Wind Prospector [24]) was downloaded on an hourly basis for 2012.

Turbines are classified as Class I, II, or III depending on the average annual wind speed, as outlined in the International Electrotechnical Commission (IEC) 61400-1 standard [25]. See Table 6 for average wind speed design details for each class.

Table 6. IEC Wind Turbine Classes

Wind Turbine Class	Average Design Windspeed (m/s)
I (High wind)	10
II (Medium wind)	8.5
III (Low wind)	7.5

The wind power equation is as follows: $Power = \frac{1}{2} \rho AV^3 C_p$, where ρ = Density of Air in kg/m^3 (about $1.225 kg/m^3$ at sea level), V = velocity in m, A = area swept by the wind turbine blades, and C_p = ratio of power extracted by wind turbine to total available in the wind resource, where 0.59 (the Betz Limit) is the theoretical maximum [26]. Because the kinetic energy available in wind is proportional to the cube of the wind velocity, a wind turbine experiencing 9 m/s winds is exposed to more than three times the force of a wind turbine experiencing 6 m/s winds. It would not be economical to design turbines for low-wind sites to the same standards as high-wind sites; therefore, different design standards were established for sites with different average levels of wind.

A wind speed-to-power conversion curve was then obtained for a Class II turbine [27]. This power curve is illustrated in Figure 5. As Class II turbines are the most common, the study team decided to calculate how changes in wind speed impact the power production of these turbines.

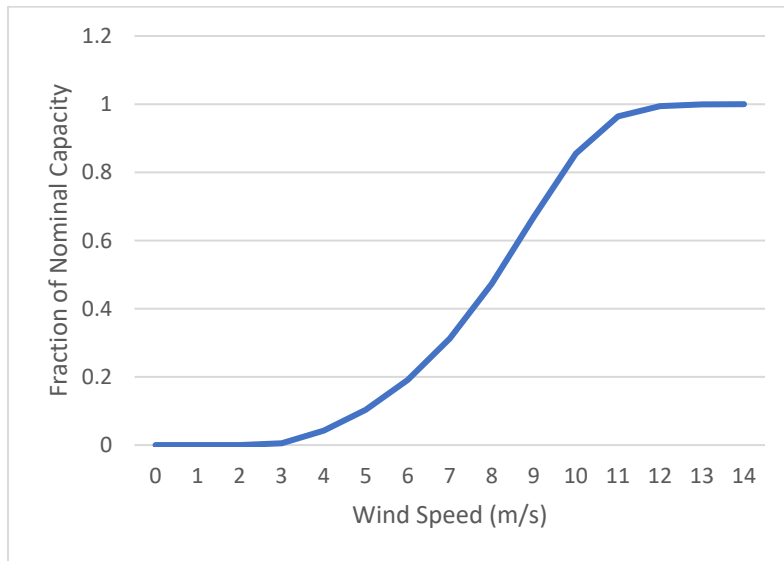


Figure 5. Power Curve for IEC Class II Turbine

Wind speed data were not obtained for each individual wind turbine – the simplifying assumption was made that since we are interested in the difference between generation at a reference wind speed and a post-climate change wind speed, it is reasonable to not take individual turbine locational differences into account.

The wind farm output in each hour was calculated using the Wind Prospector dataset for 2012 as input to the power curve in Figure 5. Since this data is for wind at 100 meters, and the NM Wind Energy Center’s turbines are at a hub height of 80 meters, the wind speed data was adjusted downwards by about 3.1% in each hour to reflect the lower wind speed at this height using a wind power-law model [28].² Next, the resulting 80 meter wind velocity was reduced in each hour by 8.7% to reflect the modeled change in the High Climate Change scenario. The wind farm power output in that scenario in each hour was then computed.

Comparing the total amount of power generated in the reference case to the High Climate Change scenario, the study team found that the 8.7% drop in wind speed in each hour led to *an overall 13% drop in wind generation output*.

The annual capacity factor calculated for the wind farm (using a single-point representation of that wind farm) was calculated at 47.7% for the reference case, and 41.2% for the High Climate Change scenario. 47.7% is an unusually high capacity factor for a wind farm and suggests that more detailed modeling may be warranted. Nevertheless, we are more interested in the difference between the two scenarios. It is reasonable that the percentage decline in power generation should be greater than the percentage decline in wind speed.

An 8.7% reduction in wind speed in each hour does not yield an 8.7% reduction in power output because the wind speed to MW output conversion formula isn’t linear. With an 8.7% drop in wind speed, the number of hours the wind speed is above 11 m/s (94.6% of full power output or greater) drops from 20.1% to 13.6% of all hours in the year. The number of hours the wind speed is 4 m/s (4.2% of full power output or less) increases from 13.6% to 16.7% of all hours in the year. In addition, the slope in the middle of the curve is quite steep – going from 7 m/s to 8 m/s causes output to increase by about 50% (from 31 MW to 47 MW for a 100-MW wind farm). An 8.7% reduction in wind speed along this section of the curve will yield a drop in power output much greater than 8.7%.

3.3. Impact of Modeled Climate Change on PNM Solar Power Generation

The potential impact of climate change on PNM solar power generation was modeled using two different methods. One method (called the “Specific” method) involved calculating the output for the Arroyo solar plant given 5-minute satellite weather data, and then adjusting the solar irradiance and increasing the ambient temperature by the climate-change-scenario amounts. Another method (called the “General” method) focused on calculating the impact of climate change on a generic solar PV facility.

The two methods arrived at the same conclusion – a 2.5% drop in solar irradiance and a 5.5 °C rise in ambient temperature (in all hours) would result in roughly a *4% drop in solar PV generation*. Based on results from the Specific method, about half of this drop is due to the decrease in solar irradiance, and about half is due to PV efficiency loss from higher ambient temperatures.

3.3.1. Climate Scenario Selection

Based on the climate modeling results given in Table 3, we see that a simulated worst-case scenario for solar PV power production would be a 2.5% drop in solar irradiance (with solar irradiance dropping from 226.7 W/m² in the reference case to 221.0 W/m² in the “Low Climate Change”

² The formula is: $U = U_r (Z / Z_r)^\alpha$, where U is the wind speed at height Z, U_r is the known wind at the reference height Z_r , and $\alpha = 0.143$ in neutral stability conditions (over land). The result is that we need to multiply the 100m wind dataset by a factor of 0.9686 to adjust for the 20m lower height of the turbines at the NM Wind Energy Center.

case), and a 5.5 °C increase in average ambient temperature (10 °C average in the reference case to 15.5 °C in the “High Climate Change” case). A great deal of uncertainty exists in these preliminary climate models, and it is possible that actual climate change impacts may be less or greater than our simulated “worst-case.” Our primary goal was to develop a methodology and framework that can be used for future analyses with more refined climate models and data.

3.3.2. Methodology – Specific Method

A single, large solar PV plant was modeled using **pvlb python**, which is a community-supported tool that allows for detailed simulation of the performance of photovoltaic energy systems [29]. It was originally ported over from the PVLIB MATLAB toolbox developed at Sandia National Laboratories and implements many of the models and methods developed there.

The location chosen for the plant was the site of the future Arroyo solar PV power plant (in McKinley County, NM – about 10 miles East of the Chaco Culture National Historical Park). Given that this plant is the largest plant approved by the NM PRC to date, and that it is a single-axis tracking plant (as all future PV plants for PNM are likely to be), the study team felt that this plant is sufficiently representative of the PV plants that will make up most of PNM’s solar PV plant capacity in the future that it can be used as a proxy for PNM solar PV plants in general.

Solar irradiance (and ambient temperature) data was downloaded from the National Solar Radiation Database (NSRDB) [30] at a five-minute resolution for the cell with coordinates latitude: 35.96°, longitude: -107.63°. This cell represents an area of 4 km² (as the spatial resolution is 2 km by 2 km). The NSRDB identifier for this cell is: 787961.

The solar irradiation data used in this model, specifically, are Diffuse Horizontal Irradiance (DHI), Direct Normal Irradiance (DNI), and Ground Horizontal Irradiance (GHI). The units for these measurements are in watts per square meter (W/m²). DHI is the amount of radiation received per square meter by a surface (not subject to any shade) that does not arrive on a direct path from the sun (in other words, light that’s been scattered by molecules in the atmosphere). DNI is the solar radiation per square meter by a surface that is always perpendicular to the light coming straight from the sun (given its current position in the sky). GHI is the total amount of shortwave radiation received from above by a surface horizontal to the ground. The relationship between these three measurements of solar irradiation is given by:

$GHI = DNI * \cos(\theta) + DHI$, where θ is the solar zenith angle (directly overhead would be $\theta = 0$) (PV Performance Modelling Collaborative, 2021)

The PV system simulated in **pvlb python** was assumed to be a single-axis tracking plant with an inverter load ratio (ILR) of 1.3. In other words, the PV panel capacity for this plant was set at 1.3 times the capacity of the AC inverter. The actual Arroyo plant will, in fact, have an ILR of 1.3, and it is likely that future solar PV plants providing power will have a similar ILR. This is because it is not economical to size the inverter at the full output capacity of the PV panels, as this full capacity would be used only for a small fraction of time. In addition, setting the inverter at a smaller size than the PV panels allows for a more even power output profile in the middle of the day. When PV panel production is greater than the inverter can accept, cloud cover that reduces PV panel production down to the inverter’s capacity has no impact on the actual AC power production from the plant.

The system size chosen was a normalized 1.3MW DC, 1MW AC system. First, the reference case was generated by loading in the five-minute solar irradiance and ambient temperature data for 2018 and running the model. The model run generated an AC power output dataset for a year (at a five-minute resolution) based on the plant type, location, and solar irradiance /ambient temperature data given.

Next, the climate change cases were generated by modifying the weather inputs to account for a Low Climate Change scenario, a High Climate Change scenario, and a Combination scenario. Specifically, GHI, DHI and DNI were reduced at all times by the amount specified in each scenario, and the temperature was increased at all times by the average ambient change specified. New model runs were made which took this modified weather data as input and produced new AC power output datasets for a year (also at a five-minute resolution). The power output for each scenario run was summed over the year, and the total annual power generated was compared with the reference run. The changes used for these scenarios, as well as the results of the model runs, are given in Table 7.

Table 7. Solar PV Scenarios and Results.

<i>Scenario</i>	<i>Change in Solar Irradiation</i>	<i>Change in Average Ambient Temperature</i>	Annual Drop in Solar Output
Low Climate Change	-2.5%	0° C	1.9%
High Climate Change	-1%	+5.5° C	2.9%
Combination	-2.5%	+5.5° C	4.1%

The Combination scenario, which posits a 2.5% drop in solar irradiation and a 5.5 °C rise in ambient temperature, led to roughly a 4% decrease in solar PV power production as compared to the reference run.

3.3.3. Methodology – General Method

In this method, the cell temperature (T_{cell}) is calculated based on the insolation (S), the ambient temperature (T_{amb}) and the normal operating cell temperature (NOCT) that is measured at 800 W/m² and 20 °C ambient as following:

$$T_{cell} = T_{amb} + (NOCT - 20) * S / 800 \text{ } ^\circ\text{C}$$

Therefore, given ambient temperature and insolation differences, the cell temperature change can be calculated as following:

$$\Delta T_{cell} = \Delta T_{amb} + (NOCT - 20) * \Delta S / 800 \text{ } ^\circ\text{C}$$

Since power-temperature coefficient (C_p - %/degree C) of a PV panel is often given based on testing data, the percentage change in output generation of the PV panels can be specified:

$$\Delta P_{out} = C_p * \Delta T_{cell}, \text{ \%}$$

Given 5.5 °C ambient temperature rise, around 2.5 % insolation reduction and -0.3% power-temperature coefficient, the overall reduction in annual generation of PV system is calculated and compared with the baseline case. The results show that PV generation drops about 4%.

This Page Left Blank

4. CLIMATE CHANGE IMPACTS ON BATTERY STORAGE

Operating temperature is one of the main factors that significantly affect the life span as well as the performance of li-ion batteries (LiB). While high temperature increases the formation and modification of the surface film on batteries' electrodes making them degrade faster, low temperature slows down the electrochemical reactions within the batteries making them less efficient. Furthermore, extremely low or high temperature can also create serious damage to LiBs. Therefore, for grid-scale battery energy storage systems (BESS), heating, venting and air conditioning (HVAC) systems are often required to maintain the battery enclosure's temperature within an operating range. Since the change in ambient temperature will impact HVAC's operation, it will also impact the overall performance of a BESS.

4.1. Impact of Temperature Change on Battery Storage

In this section, the impact of climate change is seen as the impact of ambient temperature rise on the performance and degradation of Li-ion BESS. Three scenarios of temperature rise are considered including:

- Scenario 1 - Nominal: this scenario assumes the ambient temperature would not change in the next 24 years. This is used as the baseline to evaluate the other two scenarios.
- Scenario 2 - Moderate temperature rise: this scenario considers 2-degree temperature rise in the next 24 years.
- Scenario 3: Extreme temperature rise: this scenario considers 5-degree temperature rise in the next 24 years.

Grid-scale Li-ion BESSs are required to sit outdoors by the current safety codes. Therefore, these BESSs are often packed as modules that are contained in standard shipping containers. The module size often varies with applications and manufacturers; however, in this work we model a typical 1MW/4MWh module contained within a 20-ft standardized shipping container. Just as modules can be stacked to achieve a larger system, so too this model can be scaled to model the systems of different sizes. The purpose of this model is to study the overall performance of BESS given the ambient temperature and the loading (charge/discharge) profile of the BESS. For simplification, the following assumptions are made:

- BESS alternatively charges and discharges every 12 hours
- BESS loss is purely heat loss
- Battery temperature is equal to the enclosure temperature
- The container is not insulated

The input parameters of the model are given in Table 8.

Table 8. Parameters used in HVAC modeling of BESS power consumption.

Parameters	Unit	Value
BESS Power Rating	MW	1
BESS Energy Capacity	MWh	4

Parameters	Unit	Value
LiB Specific Weight	Wh/kg	160
Mass, m	kg	25000
Round-trip Efficiency	%	90
One-way Efficiency	%	95
BESS Specific heat, c_p	J/kg.K	1000
HVAC Capacity	BTU/hr	80,000 (23,400 W)
Container Surface Area	m ²	67.63
Container Emissivity	-	0.8
HVAC Power Rating	W	8000
HVAC Duty Cycle	%	40
HVAC Max Coefficient of Performance	-	4

The container's change in temperature, ΔT (K), at each time step, i , is calculated using an energy balance:

$$\Delta T_i = \frac{\dot{E}_{in,i} - \dot{E}_{out,i}}{mc_p} \Delta t \quad (1)$$

where $\dot{E}_{in,i}$ is the heat generation (W) caused by the battery inefficiency (assumed to be lost entirely to resistive heating) during charging and discharging, $\dot{E}_{out,i}$ is the heat dissipation from radiation and conduction from the shipping container and convection via HVAC, m is the mass of the BESS and container (kg), c_p is the specific heat (J/kg-K), and $\Delta t = 1$ hr (3600 s). In the model, the HVAC is on at its rated power if the container's temperature is above 45 °C, off if the temperature is below 25 °C, and holding its status (on or off) if the temperature is decreasing below 45 °C or increasing above 25 °C. In each scenario, the model is used to simulate the container temperature at each hour throughout a year. The HVAC's energy consumption for a 4 MWh BESS is calculated accordingly and compared between different scenarios. The results are shown in Table 9.

Table 9. Modeled annual HVAC energy consumption as a function of ambient temperature rise.

Climate Scenario (ambient temperature)	HVAC Annual Energy Consumption (MWh)	HVAC Annual Energy Consumption Change (%)	Ratio (%) of HVAC Annual Energy Consumption to Annual Battery Throughput Energy ¹
Current conditions	23.5	0	1.6%
2 °C increase	25.0	12.1%	1.7%
5 °C increase	27.3	22.4%	1.9%

¹Four MWh/discharge x 365 discharges/yr = 1,460 MWh of annual battery throughput energy

As seen in Table 9, the HVAC annual energy consumption increases as the temperature rises. This is because ambient temperature rise will reduce the heat dissipation through radiation, convection, and conduction making the HVAC work harder to maintain the operating temperature range. Significant increase in HVAC energy consumption will increase the overall load of the system thereby decreasing the net impact of BESSs. However, the relative impact of an ambient temperature rise of up to ~5 °C on increased HVAC energy consumption is predicted to yield less than 1% change in the total annual battery throughput energy. Therefore, the uncertainty on increased temperatures on HVAC parasitic power consumption is not directly included in the probabilistic simulations; the uncertainty is assumed to be subsumed by the uncertainty in the capacity fade and round-trip efficiency described in the next section.

4.2. Impacts of Capacity Fade and Round-Trip Efficiency on Battery Storage

Capacity fade and round-trip efficiency can impact the available throughput energy of battery storage systems. Although not necessarily tied to climate change, this study included uncertainty in capacity fade and round-trip efficiency in the probabilistic simulations.

Capacity fade is a condition in which the total energy capacity that a battery can deliver reduces with use and is dependent on a number of factors including ambient temperature, discharge rate, and depth of discharge. Preger et al. [31] performed a multi-year test of different lithium-ion cells under varying discharge conditions and found that the number of cycles to reach an 80% capacity (20% capacity loss) ranged from only a few hundred cycles to several thousand cycles, depending on cell type and conditions. Spotnitz [32] reported that among different lithium-ion cell types, the capacity loss at 500 cycles ranged from ~12 – 24%. Based on these studies, we assume that the capacity loss of battery storage systems used by PNM may be up to 20% within a few years of deployment – before issues are identified and servicing or replacement of cells can be performed. A uniform distribution for battery capacity fade between 0 – 20% was therefore assumed and sampled for each annual realization of the hourly energy balance. This sampled value was used to reduce the total battery storage capacity prescribed in the 2040 No New Combustion scenario.

Preger et al. also evaluated the round-trip efficiency (energy out/energy in) of various lithium-ion cells and found that the initial round-trip efficiency varied between ~80% - 95%. After cycling to a capacity loss of 20%, the decrease in initial round-trip efficiency ranged from less than a few percent up to ~10% in many reported cases. Based on these studies, the round-trip efficiency (and impacts of potential degradation) for the battery systems used by PNM during any year in the probabilistic simulations was assumed to be uniformly distributed between 80 - 95%. The sampled round-trip efficiency was used to reduce amounts of energy added to the battery during any hour when supply

exceeded demand for the No New Combustion scenario. For example, if the sampled round-trip efficiency for a given year was 90%, and the energy supply exceeded demand by 10 MWh during a given hour, the energy stored during that hour for later delivery was set equal to $0.9 \times 10 \text{ MWh} = 9 \text{ MWh}$ (assuming that the total energy stored did not exceed the total nameplate capacity of all available battery storage systems, accounting for capacity fade described above).

4.3. Implementation into QuEST

QuEST is an open-source software application suite for energy storage evaluation. The latest version of QuEST includes two main applications 1) Market and 2) Behind-the-meter that are for evaluating the potential revenue of energy storage systems (ESS) providing grid and customer services. Currently, QuEST uses a linear energy flow model of an ESS that only considers round-trip loss while cycling the storage device. In other words, it ignores the impact of HVAC consumption on system performance. Therefore, the revenues produced by these applications can be much higher than they are when significant amount of energy is discounted for running the HVAC to maintain the operating temperature range.

To improve QuEST in the future, the above thermal model and uncertainties in capacity fade and round-trip efficiency can be incorporated to better capture the impact of HVAC and degradation on ESS's operation. Another way to improve QuEST is co-simulating the electrical charge/discharge behaviors of an ESS with its thermal behaviors. While the above thermal model can be used for standard shipping containers, a more sophisticated package like Energy Plus will provide more accurate results for different types of enclosures. Once the ESS model is successfully updated with a thermal model/simulation, an optimization process needs to be developed to find the optimal charge/discharge profile for an ESS given different climate patterns. The results will better inform the decision on siting and sizing ESS for a particular application given a weather pattern. The incorporation of the above model or co-simulation can be difficult as they will require QuEST to solve a non-linear problem that can be intractable.

5. PROBABILISTIC ANALYSIS OF CLIMATE CHANGE IMPACTS AND BATTERY PERFORMANCE

5.1. Modeling Approach

At each hour of the year starting at 12 AM January 1 and ending at midnight December 31, the energy, E_i (MWh), produced from all available generation sources in the 2040 No New Combustion scenario were summed, including uncertainty in intermittent wind and solar resources as impacted by climate-change modeling. In addition to variable solar and wind generation at each hour of the year, firm fixed resources (i.e., nuclear, geothermal) were added as prescribed by PNM (see Table 10). If the total generation exceeded the total load, L_i (MWh), at any hour, surplus generation was added to the battery storage (after adjustment for round-trip efficiency). If the generation was less than the load at that hour, energy was taken from battery storage. Checks were implemented to determine the minimum and maximum state of charge (SOC) of the battery storage system (in MWh) at each hour: (1) if generation was less than the load, and total SOC decreased to a value less than zero, the SOC was set to zero, and (2) if generation was greater than the load, and SOC increased to a value greater than the maximum battery storage capacity adjusted for capacity fade ($Fade$), the SOC was set equal to the maximum battery storage adjusted for capacity fade and battery round-trip efficiency (RTE). The SOC at the start of the year was assumed to be equal to 100%. The steps to calculate the SOC at each hour can therefore be summarized as follows:

$$SOC_i = SOC_{i-1} + \sum_i E_i - L_i \quad (2)$$

$$\text{If } SOC_i < 0, SOC_i = 0$$

$$\text{elseif } SOC_i > SOC_{\max}(1 - Fade_j), SOC_i = SOC_{\max}(1 - Fade_j)RTE_j$$

$$\text{elseif } \sum_i E_i - L_i > 0, SOC_i = SOC_{i-1} + \left(\sum_i E_i - L_i \right) RTE_j$$

where i is the hour of the year (1 to 8760) and j is the realization (1 to 100).

Table 10. Summary of firm fixed resources assumed for PNM 2040 No New Combustion scenario (in addition to solar and wind generation) [1].

Parameter	Value
Total energy efficiency* (MW):	95
Total demand response* (MW):	15
Total coal resources (MW):	0
Total nuclear resources (MW):	288
Total natural gas resources (MW):	0
Total geothermal resources (MW):	11
Total battery storage resource (MWh):	14,328
% battery capacity on Jan. 1 (hour 1):	100%

*Not used in probabilistic hourly energy balance.

Uncertainty distributions of wind and solar generation, battery RTE, and battery fade (Table 11) were sampled to create 100 realizations of annual energy balances for the 2040 No New Combustion scenario. Figure 6 plots the cumulative distribution functions for each of these four

stochastic parameters used in the model. All other input parameters (e.g., firm fixed resources, load) were not varied from the baseline values.

In each realization, the loss of load expectation (LOLE) was determined as the number of days (hours divided by 24) in which the SOC was equal to zero during the year. The cumulative distribution function for the LOLE was plotted for all 100 realizations. The goal was to determine if the distribution of LOLE was significantly greater than the desired value of 0.2 days/year or less with the impacts of climate change and uncertainty in battery performance. If so, a sensitivity study would be performed to determine the additional battery storage capacity required to reduce the LOLE to 0.2 days/year or less.

Table 11. Summary of uncertainty distributions in probabilistic simulations.

Parameter	Nominal Value*	Uniform Distribution	
		Minimum	Maximum
Wind generation (MWh)	-13%	-50%	+50%
Solar generation (MWh)	-4%	-50%	+50%
Battery RTE	N/A	80%	95%
Battery capacity fade	N/A	0%	10%

*The nominal value for wind and solar generation represents the impact of climate change (see Sections 3.2 and 3.3) on baseline values provided by PNM using their historical capacity factors and expected generation capacity in the 2040 No New Combustion portfolio (see Sections 5.1.1 and 5.1.2).

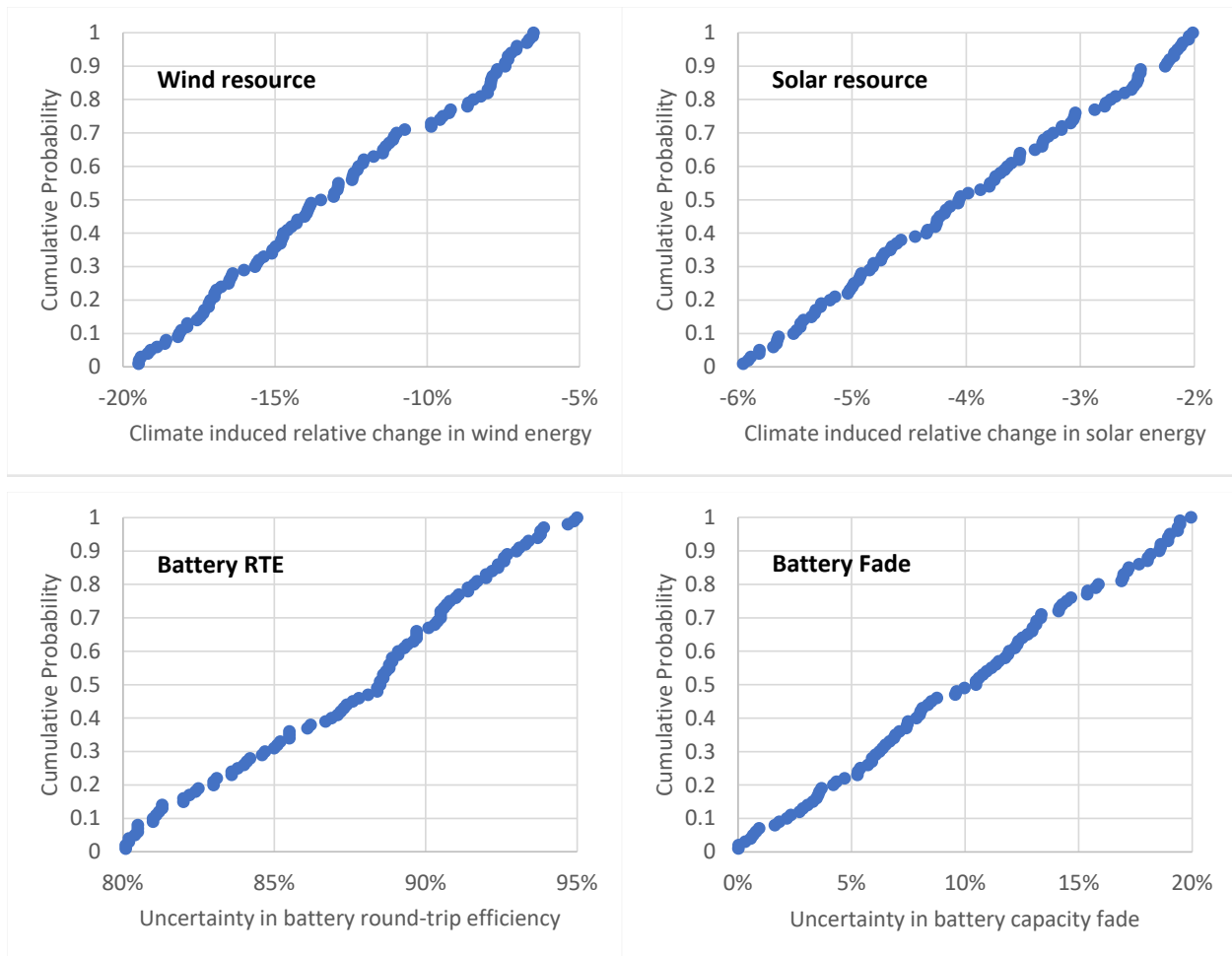


Figure 6. Cumulative distribution functions of climate-induced changes in wind and solar resources (top) and uncertainty in battery performance (RTE and capacity fade; bottom).

5.1.1. Uncertainty in Wind Energy Resources

Historical average wind-generation capacity factors for each hour of the month were reported by PNM (2013 – 2019) [1] as shown in Table 12. Figure 7 plots these hourly wind-generation capacity factors by month, which reveals that wind generation typically peaks in the late afternoon and evening hours and subsides in the morning hours. February through April are the most productive months for wind generation, while July and August are the least productive.

These hourly capacity factors were multiplied by the total expected wind generation capacity in the 2040 most cost-effective No New Combustion portfolio presented in the PNM 2020 – 2040 IRP [1] to yield baseline wind power generation values at each hour of the year (Table 13). For simplicity, the wind generation for a specific hour of any given month was assumed to be the same (e.g., the wind generation at 7 AM for each day in January was assumed to be the same; the wind generation at 3 PM for each day in July was assumed to be the same).

Uncertainty in these baseline values was accommodated by uniformly varying the baseline values by up to $\pm 50\%$ in the probabilistic simulations as summarized in Table 11. Although arbitrary, this uncertainty range was thought to be appropriate to accommodate uncertainty in not only the natural

variability in wind generation but also the uncertainty in the preliminary climate models. A sensitivity was also performed to determine the impacts of varying the uncertainty range on LOLE.

Table 12. Historical average capacity factors for PNM wind energy resources (2013 – 2019) [1].

Month	Hour																							
	1	2	3	4	5	6	7	8	9	10	11	12	13	14	15	16	17	18	19	20	21	22	23	24
1	33%	32%	33%	33%	32%	32%	32%	31%	29%	28%	28%	30%	31%	32%	33%	34%	34%	35%	37%	39%	38%	38%	36%	35%
2	39%	38%	38%	36%	35%	35%	33%	31%	27%	28%	29%	32%	35%	39%	41%	42%	43%	41%	41%	41%	42%	41%	41%	39%
3	38%	36%	34%	33%	33%	32%	29%	26%	27%	28%	29%	30%	33%	35%	36%	39%	41%	41%	40%	41%	41%	41%	40%	40%
4	38%	37%	36%	34%	32%	30%	28%	26%	27%	27%	29%	32%	35%	37%	39%	42%	44%	43%	40%	42%	45%	44%	44%	40%
5	34%	32%	31%	29%	25%	22%	19%	19%	19%	20%	22%	25%	27%	31%	34%	35%	36%	38%	36%	36%	38%	39%	39%	37%
6	33%	31%	28%	25%	24%	21%	17%	16%	14%	14%	14%	15%	17%	20%	21%	24%	25%	27%	28%	29%	33%	34%	34%	36%
7	24%	22%	21%	20%	19%	17%	14%	12%	12%	11%	10%	10%	11%	12%	14%	17%	20%	21%	24%	25%	27%	27%	26%	24%
8	21%	19%	19%	19%	18%	16%	13%	11%	10%	10%	9%	10%	12%	13%	16%	19%	21%	21%	22%	24%	25%	24%	23%	23%
9	23%	21%	20%	18%	17%	17%	16%	14%	14%	14%	15%	16%	17%	19%	21%	24%	24%	23%	24%	28%	30%	29%	28%	26%
10	29%	28%	27%	27%	25%	25%	25%	22%	21%	23%	24%	26%	28%	30%	31%	33%	33%	32%	33%	35%	35%	34%	32%	31%
11	34%	33%	32%	31%	30%	30%	30%	29%	27%	28%	30%	31%	34%	35%	37%	37%	35%	34%	36%	37%	38%	37%	36%	34%
12	33%	32%	32%	31%	31%	31%	30%	30%	27%	26%	26%	27%	29%	31%	33%	33%	31%	33%	36%	36%	35%	35%	34%	33%

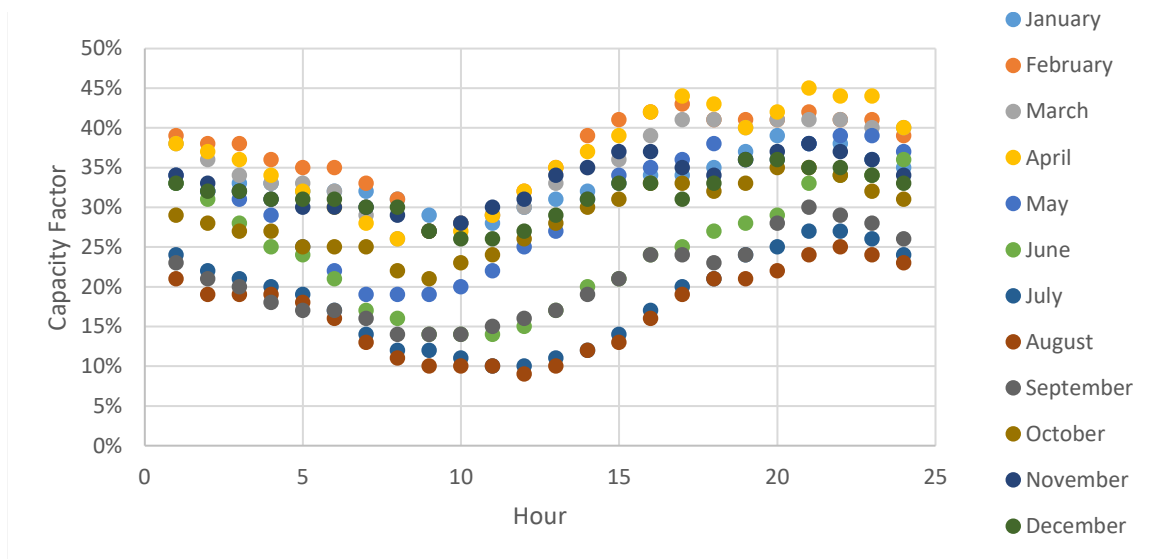


Figure 7. Plot of historical average capacity factors for PNM wind energy resources by hour and month (2013 – 2019) [1].

Table 13. Hourly baseline wind generation (MW) based on capacity factors in Table 12 and total prescribed wind generation capacity of 956 MW in the PNM IRP 2040 No New Combustion portfolio [1].

Month	Hour																							
	1	2	3	4	5	6	7	8	9	10	11	12	13	14	15	16	17	18	19	20	21	22	23	24
1	315	306	315	315	306	306	306	296	277	268	268	287	296	306	315	325	325	335	354	373	363	363	344	335
2	373	363	363	344	335	335	315	296	258	268	277	306	335	373	392	402	411	392	392	392	402	392	392	373
3	363	344	325	315	315	306	277	249	258	268	277	287	315	335	344	373	392	392	382	392	392	392	382	382
4	363	354	344	325	306	287	268	249	258	258	277	306	335	354	373	402	421	411	382	402	430	421	421	382
5	325	306	296	277	239	210	182	182	182	191	210	239	258	296	325	335	344	363	344	344	363	373	373	354
6	315	296	268	239	229	201	163	153	134	134	134	143	163	191	201	229	239	258	268	277	315	325	325	344
7	229	210	201	191	182	163	134	115	115	105	96	96	105	115	134	163	191	201	229	239	258	258	249	229
8	201	182	182	182	172	153	124	105	96	96	96	86	96	115	124	153	182	201	201	210	229	239	229	220
9	220	201	191	172	163	163	153	134	134	134	143	153	163	182	201	229	229	220	229	268	287	277	268	249
10	277	268	258	258	239	239	239	210	201	220	229	249	268	287	296	315	315	306	315	335	335	325	306	296
11	325	315	306	296	287	287	287	277	258	268	287	296	325	335	354	354	335	325	344	354	363	354	344	325
12	315	306	306	296	296	296	287	287	258	249	249	258	277	296	315	315	296	315	344	344	335	335	325	315

5.1.2. Uncertainty in Solar Energy Resources

Historical average solar-generation capacity factors for each hour of the month were reported by PNM (2013 – 2019) [1] as shown in Table 14. Figure 8 plots these hourly solar-generation capacity factors by month, which shows that solar generation peaks around the 12th hour of the day (standard time) and is highest during the spring/summer months and is lowest during the winter months.

These hourly capacity factors were multiplied by the total expected solar generation capacity in the 2040 most cost-effective No New Combustion portfolio presented in the PNM 2020 – 2040 IRP [1] to yield baseline solar power generation values at each hour of the year (Table 15). For simplicity, the solar generation for a specific hour of any given month was assumed to be the same (e.g., the solar generation at 3 PM for each day in July was assumed to be the same).

Uncertainty in these baseline values was accommodated by uniformly varying the baseline values by up to $\pm 50\%$ in the probabilistic simulations as summarized in Table 11. Although arbitrary, this uncertainty range was thought to be appropriate to accommodate uncertainty in not only the natural variability in solar generation but also the uncertainty in the preliminary climate models. A sensitivity was also performed to determine the impacts of varying the uncertainty range on LOLE.

Table 14. Historical average capacity factors for PNM solar energy resources (2013 – 2019) [1].

Month	Hour																							
	1	2	3	4	5	6	7	8	9	10	11	12	13	14	15	16	17	18	19	20	21	22	23	24
1	0%	0%	0%	0%	0%	0%	0%	2%	32%	57%	69%	74%	75%	70%	62%	46%	16%	0%	0%	0%	0%	0%	0%	0%
2	0%	0%	0%	0%	0%	0%	12%	45%	67%	77%	80%	79%	78%	71%	57%	33%	3%	0%	0%	0%	0%	0%	0%	0%
3	0%	0%	0%	0%	0%	2%	29%	58%	75%	83%	84%	83%	81%	73%	61%	41%	11%	0%	0%	0%	0%	0%	0%	0%
4	0%	0%	0%	0%	0%	14%	46%	64%	78%	85%	86%	85%	81%	74%	61%	44%	18%	0%	0%	0%	0%	0%	0%	0%
5	0%	0%	0%	0%	3%	26%	53%	68%	81%	87%	87%	86%	82%	74%	61%	46%	24%	3%	0%	0%	0%	0%	0%	0%
6	0%	0%	0%	0%	4%	28%	52%	67%	81%	88%	89%	86%	81%	72%	60%	46%	26%	5%	0%	0%	0%	0%	0%	0%
7	0%	0%	0%	0%	2%	22%	48%	65%	78%	85%	86%	83%	77%	68%	55%	40%	22%	4%	0%	0%	0%	0%	0%	0%
8	0%	0%	0%	0%	0%	14%	44%	62%	76%	84%	85%	82%	78%	68%	54%	38%	17%	1%	0%	0%	0%	0%	0%	0%
9	0%	0%	0%	0%	0%	8%	41%	61%	75%	83%	84%	82%	79%	69%	55%	35%	8%	0%	0%	0%	0%	0%	0%	0%
10	0%	0%	0%	0%	0%	2%	33%	59%	73%	80%	80%	79%	75%	67%	51%	22%	0%	0%	0%	0%	0%	0%	0%	0%
11	0%	0%	0%	0%	0%	0%	16%	47%	63%	70%	72%	71%	68%	59%	40%	8%	0%	0%	0%	0%	0%	0%	0%	0%
12	0%	0%	0%	0%	0%	0%	4%	33%	56%	65%	69%	69%	66%	57%	36%	6%	0%	0%	0%	0%	0%	0%	0%	0%

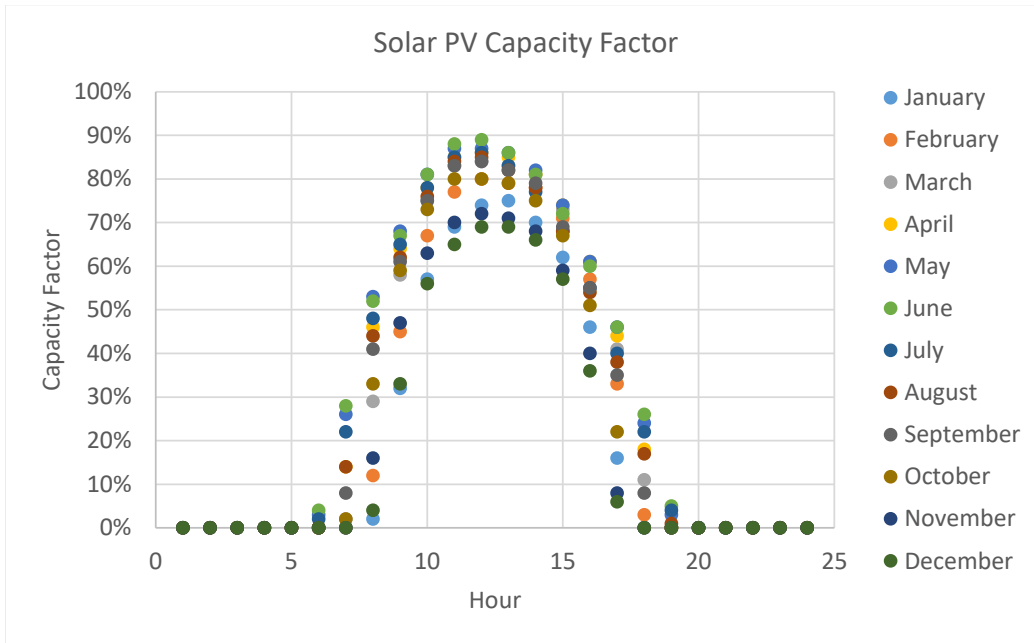


Figure 8. Plot of historical average capacity factors for PNM solar energy resources by hour and month (2013 – 2019) [1].

Table 15. Hourly baseline solar generation (MW) based on capacity factors in Table 14 and total prescribed solar generation capacity of 3,165 MW in the PNM IRP 2040 No New Combustion portfolio [1].

Month	Hour																							
	1	2	3	4	5	6	7	8	9	10	11	12	13	14	15	16	17	18	19	20	21	22	23	24
1	0	0	0	0	0	0	0	63	1013	1804	2184	2342	2374	2216	1962	1456	506	0	0	0	0	0	0	0
2	0	0	0	0	0	0	0	380	1424	2121	2437	2532	2500	2469	2247	1804	1044	95	0	0	0	0	0	0
3	0	0	0	0	0	0	63	918	1836	2374	2627	2659	2627	2564	2310	1931	1298	348	0	0	0	0	0	0
4	0	0	0	0	0	0	443	1456	2026	2469	2690	2722	2690	2564	2342	1931	1393	570	0	0	0	0	0	0
5	0	0	0	0	0	95	823	1677	2152	2564	2754	2754	2722	2595	2342	1931	1456	760	95	0	0	0	0	0
6	0	0	0	0	0	127	886	1646	2121	2564	2785	2817	2722	2564	2279	1899	1456	823	158	0	0	0	0	0
7	0	0	0	0	0	63	696	1519	2057	2469	2690	2722	2627	2437	2152	1741	1266	696	127	0	0	0	0	0
8	0	0	0	0	0	0	443	1393	1962	2405	2659	2690	2595	2469	2152	1709	1203	538	32	0	0	0	0	0
9	0	0	0	0	0	0	253	1298	1931	2374	2627	2659	2595	2500	2184	1741	1108	253	0	0	0	0	0	0
10	0	0	0	0	0	0	63	1044	1867	2310	2532	2532	2500	2374	2121	1614	696	0	0	0	0	0	0	0
11	0	0	0	0	0	0	0	506	1488	1994	2216	2279	2247	2152	1867	1266	253	0	0	0	0	0	0	0
12	0	0	0	0	0	0	0	127	1044	1772	2057	2184	2184	2089	1804	1139	190	0	0	0	0	0	0	0

5.1.3. Uncertainty in Battery Storage Resources

Table 16 shows the planned battery storage systems in PNM’s No New Combustion portfolio. The total energy capacity (MWh) of each system was calculated as the product of the power capacity (MW) and storage duration of each system. The total energy storage capacity was used in the hourly energy balance calculations. Uncertainty in the battery storage capacity and performance was included by sampling the capacity fade and RTE for each annual realization using the uncertainty distributions in Table 11 and applying those to the conditions in Eq. (2).

Table 16. Summary of planned battery storage systems in PNM’s No New Combustion, most cost-effective portfolio [1].

Storage System*	Nameplate Capacity (MW)			
	2021	2022	2030	2040
Arroyo Storage ESA (MW)	0	150	150	150
Jicarilla Storage ESA (MW)	0	20	20	20
Rockmont Storage ESA (MW)	0	30	30	30
San Juan Storage ESA (MW)	0	100	100	100
New Lithium Ion Battery (4 hr) (MW)	0	0	508	1025
New Lithium Ion Battery (8 hr) (MW)	0	0	262	391
New Flow Battery (10 hr) (MW)	0	0	0	590
New Pumped Storage (MW)	0	0	0	0
Total storage capacity (MWh)	0	1200	5328	14328

*ESA (Energy Storage Agreement) storage systems were assumed to be 4-hour Li-ion batteries for calculating energy capacity

5.1.4. Annual Energy Load

PNM provided the reference forecast for hourly electricity loads to Sandia. For each month, the loads at a particular hour of each day were averaged. Therefore, the hourly load for a particular time each day during a given month were assumed to be the same. For example, the load at 10 AM for each day in March was assumed to be the same. Table 17 shows the average hourly loads (MW) by month for the 2040 reference forecast. The 2040 loads were approximately 6% higher than the 2020 reference loads.

Table 17. Average hourly loads (MW)* by month using reference 2040 forecast (PNM 2020 – 2040 IRP [1]).

Hourly Load (MW) by Month												
Hour	Jan	Feb	Mar	Apr	May	Jun	Jul	Aug	Sep	Oct	Nov	Dec
1	1014	941	888	853	904	1090	1186	1120	975	874	942	1019
2	963	894	842	808	846	1005	1097	1045	910	829	895	970
3	940	871	820	782	812	950	1042	994	871	805	871	943
4	932	862	814	769	793	916	1007	965	848	794	864	935
5	947	880	826	780	798	908	999	962	850	809	883	951
6	999	933	878	833	843	940	1032	1002	888	859	937	1000
7	1090	1027	966	912	880	956	1053	1061	960	951	1020	1079
8	1126	1037	984	915	885	980	1080	1072	960	982	1023	1103
9	1086	981	932	870	859	988	1093	1070	942	940	959	1061
10	1021	920	868	821	835	1013	1123	1079	927	874	887	988
11	956	855	803	774	817	1044	1167	1107	920	810	826	918
12	906	811	761	750	821	1091	1234	1161	940	775	788	875
13	889	801	749	749	842	1155	1310	1225	978	775	789	861
14	900	813	751	762	884	1235	1389	1307	1036	799	820	879

Hourly Load (MW) by Month												
Hour	Jan	Feb	Mar	Apr	May	Jun	Jul	Aug	Sep	Oct	Nov	Dec
15	935	846	773	784	940	1323	1481	1405	1125	848	886	934
16	995	898	817	833	1013	1413	1579	1506	1231	927	969	1015
17	1093	987	898	915	1102	1505	1671	1608	1341	1031	1073	1127
18	1234	1105	1005	1008	1201	1589	1742	1684	1436	1142	1204	1279
19	1318	1222	1106	1086	1263	1632	1761	1701	1458	1214	1252	1332
20	1323	1236	1167	1133	1282	1629	1740	1668	1457	1247	1254	1336
21	1311	1226	1183	1181	1303	1606	1715	1650	1428	1224	1247	1331
22	1254	1173	1128	1121	1241	1528	1629	1543	1325	1148	1190	1276
23	1156	1080	1036	1018	1120	1369	1468	1382	1190	1047	1099	1188
24	1070	996	946	922	999	1209	1307	1233	1064	947	1006	1088

*Hourly loads in MW are equivalent to hourly energy requirements in MWh.

5.2. Modeling Results

Results showed that the baseline LOLE (assuming 100% battery performance including 100% RTE and no capacity fade) was 0 days/year with the assumed generation resources, loads, and an assumed initial battery SOC (hour 1 of the year) of 100%.³ The probabilistic simulations using uncertainty distributions summarized in Table 11 yielded a median LOLE of ~2 days/year and a 95th percentile of LOLE of ~8 days/year. A sensitivity study that reduced the uncertainty distribution for the wind and solar generation from +/- 50% to +/- 25% about the nominal climate-impacted value yielded a similar median LOLE of ~2 days/year and a 95th percentile of LOLE of ~7 days/year. Figure 9 shows the cumulative distribution functions of LOLE for the probabilistic simulations.

Figure 10 shows the results of a rank-regression analysis to determine the impact of uncertainties in the wind and solar resources and battery performance (RTE and capacity fade) on the LOLE using the +/- 50% uniform uncertainty distribution for wind and solar resources. Results show that the battery RTE was the most significant parameter that impacted LOLE, followed by solar resource, wind resource, and battery fade. Figure 11 shows the incremental coefficients of determination for the uncertainty parameters. Uncertainty in the battery RTE yielded the greatest variability in the LOLE, followed by solar resource, wind resource, and battery fade. Similar results were obtained when a +/- 25% uncertainty distribution was assumed.

A sensitivity study was performed to determine how much battery storage capacity was required to reduce the LOLE to 0.2 days/year. In order to reduce the median (50th percentile) LOLE to 0.2 day/year, the battery storage capacity had to be increased from the baseline value of 14,328 MWh to ~25,000 – 30,000 MWh, about a factor of two higher than the baseline value assumed by PNM. In order to reduce the 95th percentile of LOLE to 0.2 day/year, the battery storage capacity had to be increased to ~100,000 MWh (Figure 12), about a factor of seven times higher than the baseline value.

³ An initial SOC of 0% increased the LOLE to 0.33 days/year for the baseline case. An initial SOC of 10% resulted in an LOLE of 0.2 days/year.

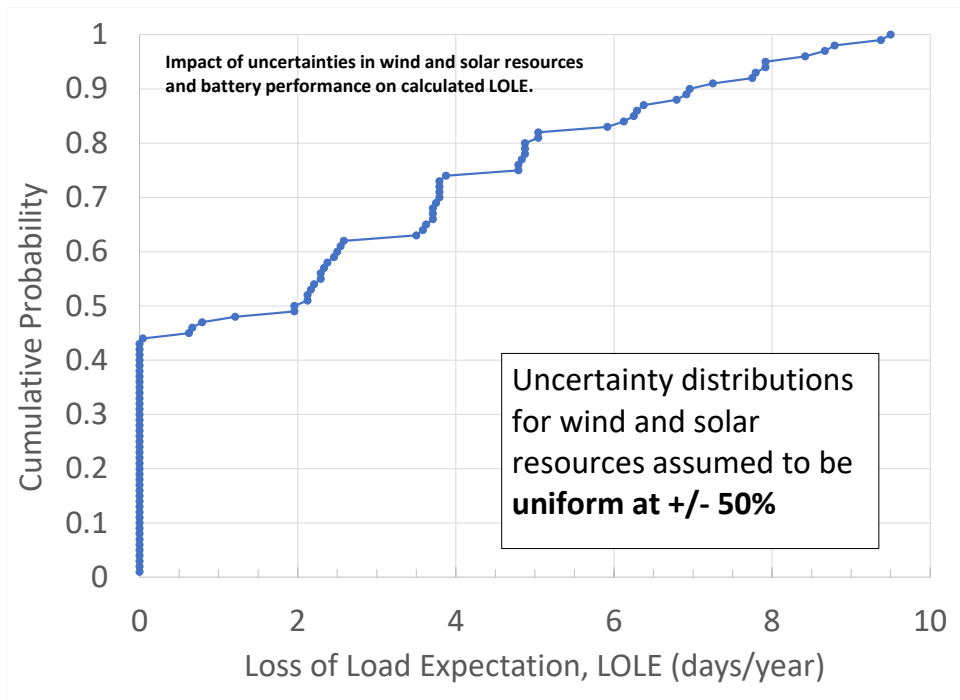
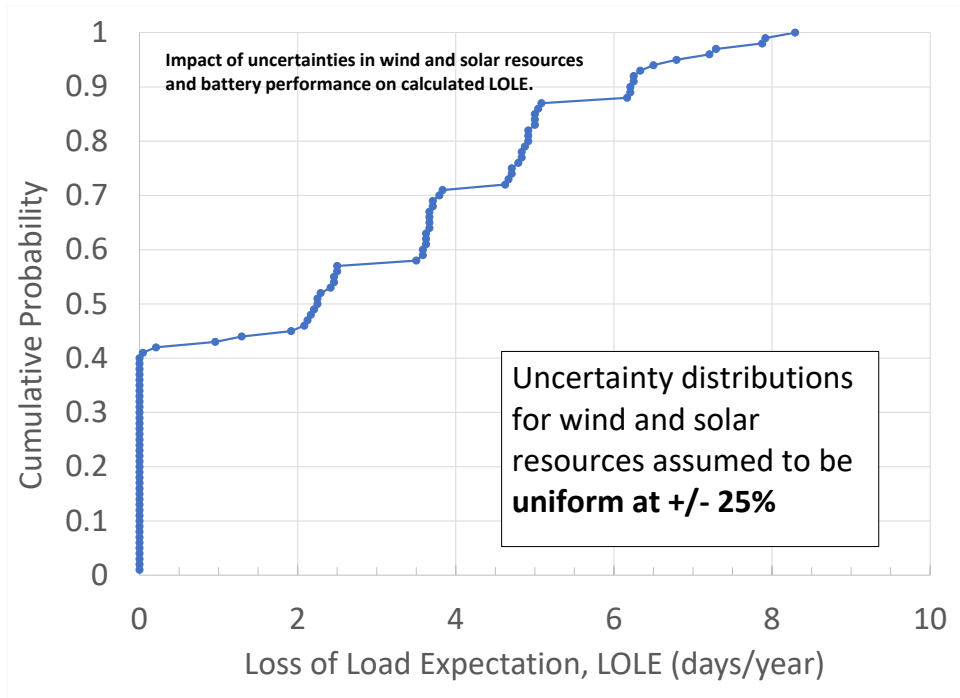


Figure 9. Cumulative probability of loss of load expectation (LOLE) with inclusion of solar and wind resource uncertainty resulting from climate change and uncertainty in battery performance. Uniform distributions of $\pm 25\%$ (top) and $\pm 50\%$ (bottom) were assumed for the solar, wind, and battery performance uncertainty distributions.

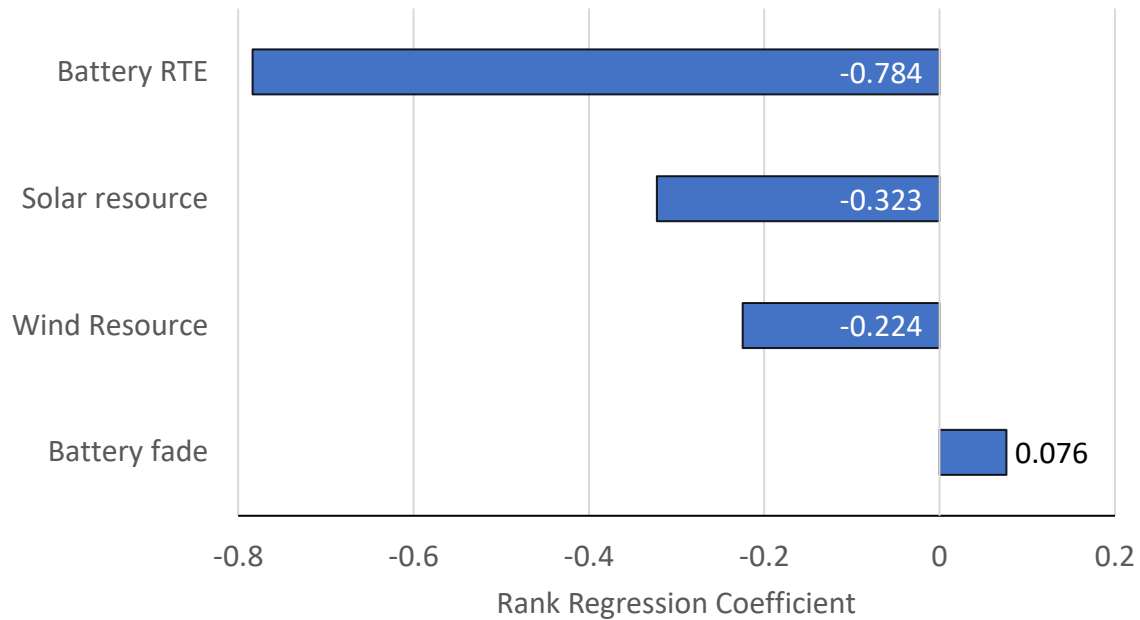


Figure 10. Impact of uncertainties in solar and wind resources and battery performance resulting from climate change on LOLE. Standardized rank regression coefficients are shown. Uniform distributions of $\pm 50\%$ were assumed for the solar, wind, and battery performance uncertainty distributions.

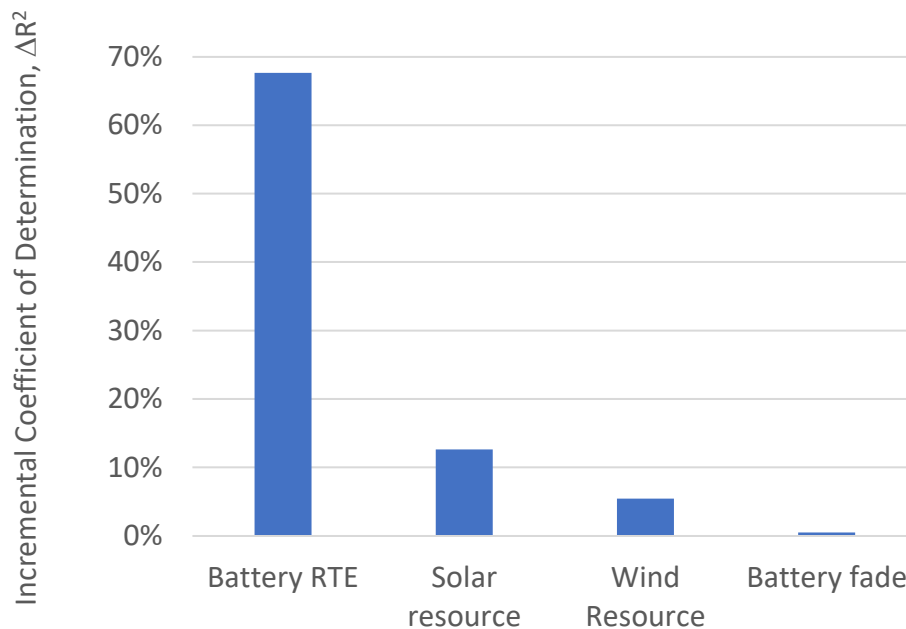


Figure 11. Impact of uncertainties in solar and wind resources and battery performance resulting from climate change on LOLE variability. Incremental coefficients of determination are shown. Uniform distributions of $\pm 50\%$ were assumed for the solar, wind, and battery performance uncertainty distributions.

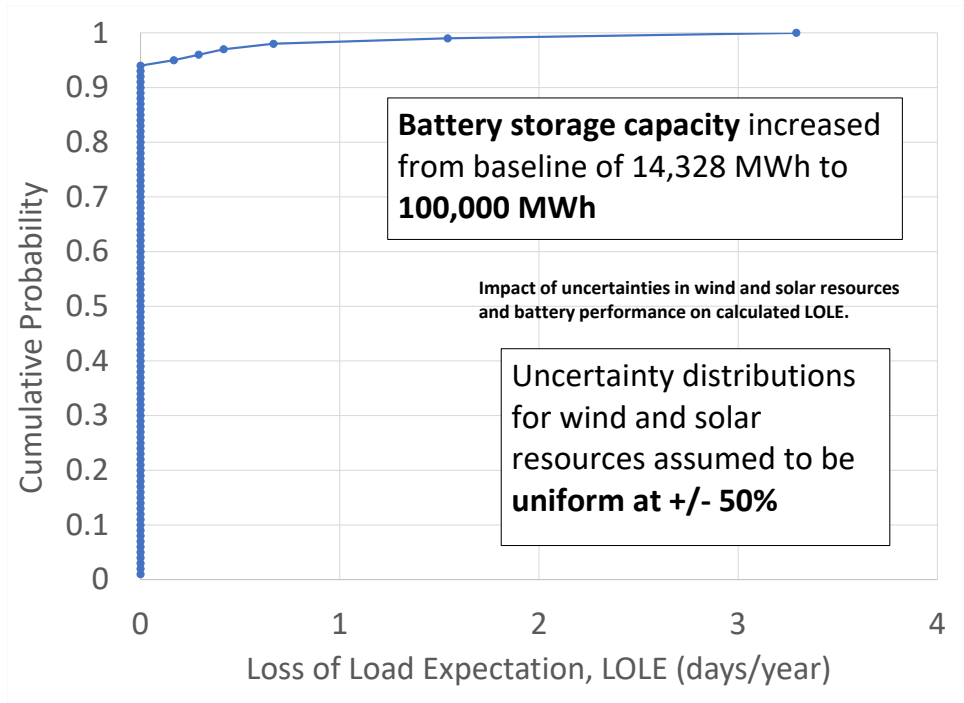


Figure 12. Cumulative probability of LOLE with increased battery storage capacity of 100,000 MWh (from 14,328 MWh) resulting in a 95% confidence that the LOLE would be ≤ 0.2 days/year for assumed uncertainties in solar, wind, and battery performance.

This Page Left Blank

6. CONCLUSION AND RECOMMENDATIONS

New Mexico's Energy Transition Act (ETA) requires power utilities in New Mexico to increase their share of carbon-free electricity generation to 50% by 2030, 80% by 2040, and 100% by 2045. According to its 2020 Integrated Resource Plan, PNM's plan is to rely heavily on utility-scale PV and wind generation with battery energy storage to meet these requirements in the most cost-effective portfolio with no new combustion. The objective of this work was to develop a methodology to evaluate the potential impacts of climate change on wind and solar resources, as well as uncertainties in battery performance, on the annual LOLE.

6.1. Climate Modeling

Three CMPI6 simulations from the E3SM model were chosen for this study to evaluate potential climate-change impacts on wind and solar resources: 'piControl', 'historical', and 'SSP585'. Each of these simulations were chosen to represent a 'no climate change' scenario, a 'low climate change' scenario, and a 'high climate change' scenario, respectively. Surface wind speeds, surface temperatures, and surface downwelling shortwave radiation values were calculated over the state of New Mexico's domain based on temporal and spatial averages from each of the three simulations. Surface temperature over New Mexico was calculated to have a 5.5 °C increase between the 'no climate change' and 'high climate change' scenarios. The solar irradiance was projected to decrease by 2.5% in the worst-case scenario, and the surface wind speed was calculated to decrease by 8.7%. There was much variability in the averaged variables representing the three climate change scenarios, and it is inconclusive in this study, as well as others, for trends in surface downwelling shortwave radiation and surface wind speeds. The uncertainty and variability within these calculations is transferred to the probabilistic energy storage and production models. Future work could include, but is not limited to, bounding the uncertainty and variability of the climate change scenarios by using higher resolution models, increasing the number of global models used, and assessing trends from other simulation scenarios.

6.2. Climate Impacts on Wind and Solar Energy Resources

A climate-induced 8.7% decrease in average hourly wind speed resulted in a calculated annual decrease in wind energy generation of 13%. Wind generation calculations used a single point for wind speed in order to approximate the impact of a decrease in wind speed on multiple turbines in a wind farm. A 2.5% drop in solar irradiation and a 5.5 °C rise in ambient temperature (in all hours) resulted in roughly a 4% drop in solar PV generation using a large, single-axis PV plant. About half of this drop was due to the decrease in solar irradiation, and about half was due to PV efficiency loss from higher ambient temperatures.

6.3. Climate Impacts on Battery Performance and Storage

Battery performance, life span, and safety are dependent on thermal management. Therefore, battery energy storage systems must be placed inside controlled environments where the temperature is carefully managed. As the ambient temperature rises due to climate change, more energy will be consumed by HVAC systems to maintain the temperature within recommended operating ranges. Modeling results showed that the expected increase in annual energy consumption was less than 2% for climate-induced temperature increases up to 5 °C. Therefore, the potential impact of additional HVAC power consumption was subsumed in the uncertainty of battery round-trip efficiency and capacity fade. Based on reported literature data, the battery RTE was assumed to be uniformly

distributed between 80 – 95%, and the battery capacity fade was assumed to be uniformly distributed between 0 – 20% for any year following installation.

6.4. Energy Balance and Climate Impacts on LOLE

An energy balance was applied to each hour of the year for the most cost-effective portfolio assuming a No New Combustion scenario in 2040 from the PNM 2020 – 2040 IRP, which included nearly 1,000 MW of variable wind energy and ~3,200 MW of variable solar energy capacity. If energy generation exceeded load at any hour, the surplus generation was added to the battery storage system (nameplate capacity ~2,300 MW). Results showed that the baseline LOLE (assuming 100% battery performance including 100% RTE and no capacity fade) was 0 days/year with the assumed generation resources, loads, and an assumed initial battery SOC (hour 1 of the year) of 100%.

In addition to the baseline model, a probabilistic model was developed to evaluate the impacts of climate-induced uncertainties in wind and solar resources, battery RTE, and battery capacity fade on the LOLE. The probabilistic simulations using uncertainty distributions summarized in Table 11 yielded a median LOLE of ~2 days/year and a 95th percentile of LOLE of ~8 days/year. A rank regression analysis revealed that the battery RTE was the most significant parameter that impacted LOLE, followed by solar resource, wind resource, and battery fade. In order to reduce the median (50th percentile) LOLE to 0.2 day/year, the battery storage capacity had to be increased from the baseline value of 14,328 MWh to ~25,000 – 30,000 MWh, about a factor of two higher than the baseline value assumed by PNM. In order to reduce the 95th percentile of LOLE to 0.2 day/year, the battery storage capacity had to be increased to ~100,000 MWh, about a factor of seven times higher than the baseline value assumed by PNM.

Factors such as reliability, maintenance, and uncertainty in load were not included in the models. The primary objective was to develop and demonstrate a method and framework to probabilistically model hourly energy balances that accounted for uncertainties in variable resource generation, battery performance, and climate impacts. These methods can be utilized in future IRPs and models to gain confidence in future resource portfolios that can achieve 100% carbon-free electricity production by 2045 as prescribed in NM's Energy Transition Act.

REFERENCES

- [1] Phillips, N., M. Reiman, D. Brunton, S. Gutierrez, and J. Heslop, 2021, PNM 2020 - 2040 Integrated Resource Plan, Public Service Company of New Mexico, Albuquerque, NM. January 29, 2021 <https://www.pnmforwardtogether.com/irp>.
- [2] Burrows, S.M., M. Maltrud, X. Yang, Q. Zhu, N. Jeffery, X. Shi, D. Ricciuto, S. Wang, G. Bisht, J. Tang, J. Wolfe, B.E. Harrop, B. Singh, L. Brent, S. Baldwin, T. Zhou, P. Cameron-Smith, N. Keen, N. Collier, M. Xu, E.C. Hunke, S.M. Elliott, A.K. Turner, H. Li, H. Wang, J.-C. Golaz, B. Bond-Lamberty, F.M. Hoffman, W.J. Riley, P.E. Thornton, K. Calvin, and L.R. Leung, 2020, The DOE E3SM v1.1 Biogeochemistry Configuration: Description and Simulated Ecosystem-Climate Responses to Historical Changes in Forcing, *Journal of Advances in Modeling Earth Systems*, **12**(9), p. e2019MS001766.
- [3] Eyring, V., S. Bony, G.A. Meehl, C.A. Senior, B. Stevens, R.J. Stouffer, and K.E. Taylor, 2016, Overview of the Coupled Model Intercomparison Project Phase 6 (CMIP6) experimental design and organization, *Geosci. Model Dev.*, **9**(5), p. 1937-1958.
- [4] Golaz, J.-C., P.M. Caldwell, L.P.V. Roedel, M.R. Petersen, Q. Tang, J.D. Wolfe, G. Abeshu, V. Anantharaj, X.S. Asay-Davis, D.C. Bader, S.A. Baldwin, G. Bisht, P.A. Bogenschutz, M. Branstetter, M.A. Brunke, S.R. Brus, S.M. Burrows, P.J. Cameron-Smith, A.S. Donahue, M. Deakin, R.C. Easter, K.J. Evans, Y. Feng, M. Flanner, J.G. Foucar, J.G. Fyke, B.M. Griffin, C. Hannay, B.E. Harrop, M.J. Hoffman, E.C. Hunke, R.L. Jacob, D.W. Jacobsen, N. Jeffery, P.W. Jones, N.D. Keen, S.A. Klein, V.E. Larson, L.R. Leung, H.-Y. Li, W. Lin, W.H. Lipscomb, P.-L. Ma, S. Mahajan, M.E. Maltrud, A. Mametjanov, J.L. McClean, R.B. McCoy, R.B. Neale, S.F. Price, Y. Qian, P.J. Rasch, J.E.J.R. Eyre, W.J. Riley, T.D. Ringler, A.F. Roberts, E.L. Roesler, A.G. Salinger, Z. Shaheen, X. Shi, B. Singh, J. Tang, M.A. Taylor, P.E. Thornton, A.K. Turner, M. Veneziani, H. Wan, H. Wang, S. Wang, D.N. Williams, P.J. Wolfram, P.H. Worley, S. Xie, Y. Yang, J.-H. Yoon, M.D. Zelinka, C.S. Zender, X. Zeng, C. Zhang, K. Zhang, Y. Zhang, X. Zheng, T. Zhou, and Q. Zhu, 2019, The DOE E3SM Coupled Model Version 1: Overview and Evaluation at Standard Resolution, *Journal of Advances in Modeling Earth Systems*, **11**(7), p. 2089-2129.
- [5] Tebaldi, C., K. Debeire, V. Eyring, E. Fischer, J. Fyfe, P. Friedlingstein, R. Knutti, J. Lowe, B. O'Neill, B. Sanderson, D. van Vuuren, K. Riahi, M. Meinshausen, Z. Nicholls, K.B. Tokarska, G. Hurtt, E. Kriegler, J.-F. Lamarque, G. Meehl, R. Moss, S.E. Bauer, O. Boucher, V. Brovkin, Y.-H. Byun, M. Dix, S. Gualdi, H. Guo, J.G. John, S. Kharin, Y. Kim, T. Koshiro, L. Ma, D. Olivié, S. Panickal, F. Qiao, X. Rong, N. Rosenbloom, M. Schupfner, R. Séférian, A. Sellar, T. Semmler, X. Shi, Z. Song, C. Steger, R. Stouffer, N. Swart, K. Tachiiri, Q. Tang, H. Tatebe, A. Voldoire, E. Volodin, K. Wyser, X. Xin, S. Yang, Y. Yu, and T. Ziehn, 2021, Climate model projections from the Scenario Model Intercomparison Project (ScenarioMIP) of CMIP6, *Earth System Dynamics*, **12**(1), p. 253-293.
- [6] Solaun, K. and E. Cerdá, 2019, Climate change impacts on renewable energy generation. A review of quantitative projections, *Renewable and Sustainable Energy Reviews*, **116**, p. 109415.
- [7] Craig, M.T., S. Cohen, J. Macknick, C. Draxl, O.J. Guerra, M. Sengupta, S.E. Haupt, B.-M. Hodge, and C. Brancucci, 2018, A review of the potential impacts of climate change on bulk power system planning and operations in the United States, *Renewable and Sustainable Energy Reviews*, **98**, p. 255-267.
- [8] Craig, M.T., I.L. Carreño, M. Rossol, B.-M. Hodge, and C. Brancucci, 2019, Effects on power system operations of potential changes in wind and solar generation potential under climate change, *Environmental Research Letters*, **14**(3), p. 034014.

- [9] Losada Carreño, I., M.T. Craig, M. Rossol, M. Ashfaq, F. Batibeniz, S.E. Haupt, C. Draxl, B.-M. Hodge, and C. Brancucci, 2020, Potential impacts of climate change on wind and solar electricity generation in Texas, *Climatic Change*, **163**(2), p. 745-766.
- [10] Haupt, S.E., J. Copeland, W.Y.Y. Cheng, Y. Zhang, C. Ammann, and P. Sullivan, 2016, A Method to Assess the Wind and Solar Resource and to Quantify Interannual Variability over the United States under Current and Projected Future Climate, *Journal of Applied Meteorology and Climatology*, **55**(2), p. 345-363.
- [11] Mearns, L., S. McGinnis, D. Korytina, R. Arritt, S. Biner, M. Bukovsky, H.-I. Chang, O. Christensen, D. Herzmann, Y. Jiao, S. Khari, M. Lazare, G. Nikulin, M. Qian, J. Scinocca, K. Winger, C. Castro, A. Frigon, and W. Gutowski, *The NA-CORDEX dataset*, 2017, UCAR/NCAR.
- [12] Skamarock, W., J. Klemp, J. Dudhia, D. Gill, D. Barker, W. Wang, X.-Y. Huang, and M. Duda, 2008, A Description of the Advanced Research WRF Version 3, UCAR/NCAR, 1002 KB 2008-06
- [13] Chen, L., 2020, Impacts of climate change on wind resources over North America based on NA-CORDEX, *Renewable Energy*, **153**, p. 1428-1438.
- [14] Pryor, S.C., R.J. Barthelmie, M.S. Bukovsky, L.R. Leung, and K. Sakaguchi, 2020, Climate change impacts on wind power generation, *Nature Reviews Earth & Environment*, **1**(12), p. 627-643.
- [15] Crook, J.A., L.A. Jones, P.M. Forster, and R. Crook, 2011, Climate change impacts on future photovoltaic and concentrated solar power energy output, *Energy & Environmental Science*, **4**(9), p. 3101-3109.
- [16] Folini, D., T.N. Dallafior, M.Z. Hakuba, and M. Wild, 2017, Trends of surface solar radiation in unforced CMIP5 simulations, *Journal of Geophysical Research: Atmospheres*, **122**(1), p. 469-484.
- [17] Haupt, S.E., B. Kosović, T. Jensen, J.K. Lazo, J.A. Lee, P.A. Jiménez, J. Cowie, G. Wiener, T.C. McCandless, M. Rogers, S. Miller, M. Sengupta, Y. Xie, L. Hinkelman, P. Kalb, and J. Heiser, 2018, Building the Sun4Cast System: Improvements in Solar Power Forecasting, *Bulletin of the American Meteorological Society*, **99**(1), p. 121-136.
- [18] Huber, I., L. Bugliaro, M. Ponater, H. Garny, C. Emde, and B. Mayer, 2016, Do climate models project changes in solar resources?, *Solar Energy*, **129**, p. 65-84.
- [19] Chen, L., 2021, Uncertainties in solar radiation assessment in the United States using climate models, *Climate Dynamics*, **56**(1), p. 665-678.
- [20] Jackson, N.D. and T. Gunda, 2021, Evaluation of extreme weather impacts on utility-scale photovoltaic plant performance in the United States, *Applied Energy*, **302**, p. 117508.
- [21] Jiménez, P.A., S. Alessandrini, S.E. Haupt, A. Deng, B. Kosovic, J.A. Lee, and L.D. Monache, 2016, The Role of Unresolved Clouds on Short-Range Global Horizontal Irradiance Predictability, *Monthly Weather Review*, **144**(9), p. 3099-3107.
- [22] Wang, M., P. Ullrich, and D. Millstein, 2020, Future projections of wind patterns in California with the variable-resolution CESM: a clustering analysis approach, *Climate Dynamics*, **54**(3), p. 2511-2531.
- [23] Millstein, D., J. Solomon-Culp, M. Wang, P. Ullrich, and C. Collier, 2019, Wind energy variability and links to regional and synoptic scale weather, *Climate Dynamics*, **52**(7), p. 4891-4906.
- [24] National Renewable Energy Laboratory. *Wind Prospector*. [Accessed 2021]; Available from: <https://maps.nrel.gov/wind-prospector>.
- [25] International Electrotechnical Commission, 2005, Wind turbines - Part 1: Design requirements, IEC 61400-1:2005, <https://webstore.iec.ch/publication/5426>.

- [26] Kalmikov, A., K. Dykes, and K. Araujo, Wind Power Fundamentals, MIT, <https://web.mit.edu/windenergy/windweek/Presentations/Wind%20Energy%20101.pdf>.
- [27] King, J., A. Clifton, and B.M. Hodge, 2014, Validation of Power Output for the WIND Toolkit, National Renewable Energy Laboratory, NREL/TP-5D00-61714, Golden, CO. <https://www.nrel.gov/docs/fy14osti/61714.pdf>.
- [28] Newman, J.F. and P.M. Klein, 2014, The Impacts of Atmospheric Stability on the Accuracy of Wind Speed Extrapolation Methods, *Resources*, **3**(1), p. 81-105.
- [29] Holmgren, W.F., C.W. Hansen, and M.A. Mikofski, 2018, pvlib python: a python package for modeling solar energy systems, *The Journal of Open Source Software*, **3**(29).
- [30] Sengupta, M., Y. Xie, A. Lopez, A. Habte, G. Maclaurin, and J. Shelby, 2018, The National Solar Radiation Data Base (NSRDB), *Renewable and Sustainable Energy Reviews*, **89**, p. 51-60.
- [31] Preger, Y., H.M. Barkholtz, A. Fresquez, D.L. Campbell, B.W. Juba, J. Romàn-Kustas, S.R. Ferreira, and B. Chalamala, 2020, Degradation of Commercial Lithium-Ion Cells as a Function of Chemistry and Cycling Conditions, *Journal of The Electrochemical Society*, **167**(12), p. 120532.
- [32] Spotnitz, R., 2003, Simulation of capacity fade in lithium-ion batteries, *Journal of Power Sources*, **113**(1), p. 72-80.

This Page Left Blank

DISTRIBUTION

Email—Internal

Name	Org.	Sandia Email Address
Technical Library	01911	sanddocs@sandia.gov



**Sandia
National
Laboratories**

Sandia National Laboratories is a multimission laboratory managed and operated by National Technology & Engineering Solutions of Sandia LLC, a wholly owned subsidiary of Honeywell International Inc. for the U.S. Department of Energy's National Nuclear Security Administration under contract DE-NA0003525.